

SENSITIVITY OF p PROCESS NUCLEOSYNTHESIS TO NUCLEAR REACTION RATES IN A 25 SOLAR MASS SUPERNOVA MODEL

W. RAPP, J. GÖRRES, AND M. WIESCHER

University of Notre Dame, Department of Physics & Joint Institute of Nuclear Astrophysics, 225 Nieuwland Science Hall, Notre Dame, IN 46556, USA

H. SCHATZ

Department of Physics and Astronomy, National Superconducting Cyclotron Laboratory & Joint Institute of Nuclear Astrophysics, Michigan State University, East Lansing, MI 48824, USA

F. KÄPPELER

Forschungszentrum Karlsruhe, Institut für Kernphysik, P.O. Box 3640, 76021 Karlsruhe, Germany
Draft version July 12, 2018

ABSTRACT

The astrophysical p process, which is responsible for the origin of the proton rich stable nuclei heavier than iron, was investigated using a full nuclear reaction network for a type II supernova explosion when the shock front passes through the O/Ne layer. Calculations were performed with a multi-layer model adopting the seed of a pre-explosion evolution of a 25 solar mass star. The reaction flux was calculated to determine the main reaction path and branching points responsible for synthesizing the proton rich nuclei. In order to investigate the impact of nuclear reaction rates on the predicted p -process abundances, extensive simulations with different sets of collectively and individually modified neutron-, proton-, α -capture and photodisintegration rates have been performed. These results are not only relevant to explore the nuclear physics related uncertainties in p -process calculations but are also important for identifying the strategy and planning of future experiments.

Subject headings: nuclear reactions, nucleosynthesis, abundances — supernovae: general

1. INTRODUCTION

The majority of the observed heavy nuclei above iron have been produced by neutron induced nucleosynthesis processes such as the slow neutron capture process (s process) in low mass AGB stars and massive red giant stars and the rapid neutron capture process (r process) in the supernova shock front (Käppeler et al. 1989).

In nature, 35 nuclei can be found on the neutron deficient side of the valley of stability ranging from ^{74}Se to ^{196}Hg , which are shielded against production by neutron capture processes. For the nucleosynthesis of these isotopes the p process has been proposed as the most likely scenario. The nature of the p process is still under debate and it is possible that it represents different independent nucleosynthesis scenarios. The contribution from charged particle induced nuclear reactions are most likely negligible because the high Coulomb barrier reduces the associated reaction rates significantly, though the possibility of some contribution to the lightest p -nuclei cannot be entirely excluded (Schatz et al. 1998; Jordan & Meyer 2004). In its current interpretation the p process is described as γ induced photodisintegration of stable nuclei in the shock front of type II supernovae (Woosley & Howard 1978; Rayet et al. 1990) or alternatively in the deflagration flame of a type I supernova detonation (Howard et al. 1991). More recently pre-explosive sites for the p -process have been suggested in the O-Ne burning zone of massive stars. This feature emerges in one dimensional stellar evolution models (Rauscher et al. 2002) and also in two dimensional simulations of convective oxygen rich burn-

ing zones. However, in the two dimensional study the calculation of the associated nucleosynthesis pattern has been limited to a one dimensional model adaptation and does not yet include quantitative abundance predictions (Baleisis & Arnett 2001). Supercritical accretion disks associated with jets in supernovae have also been proposed as a possible scenario (Fujimoto et al. 2003).

The bulk of p isotopes represents a small fraction of the total abundance and is presently based on the analysis of meteorite data (Anders et al. 1989). This is illustrated in Fig. 1, where the abundance distributions are compared for all those heavy isotopes, which can be entirely ascribed to a specific production process. In most cases the predicted p -process abundances agree within a factor of three with the observed values (Lambert 1992; Meyer 1994; Rayet et al. 1995). However, there still are significant discrepancies for the light p nuclei $^{92,94}\text{Mo}$ and $^{96,98}\text{Ru}$, which are largely overabundant compared to the model predictions, as well as for the Dy and Gd p -isotopes in mass region $A = 150 - 160$. Such discrepancies are reviewed in more detail in Arnould & Goriely (2003), who give a comprehensive review of the present interpretation and questions related to p -process nucleosynthesis. While Arnould & Goriely (2003) discuss the global aspects of p -process nucleosynthesis, the present work concentrates on the nuclear physics related uncertainties in p -process model predictions and in particular on the identification of critical p -process reaction rates, which are most important for further experimental studies.

The presently favored scenario for the p process are

type II supernova (SN) explosions (Arnould & Goriely 2003; Hayakawa et al. 2004). The emerging shock front causes a rapid increase in temperature and density in the different layers of the pre-supernova star. As displayed in Fig. 2 peak temperatures between $1.7 < T_9 < 3.3$ are reached in the Ne/O layer of the presupernova envelope (Rayet et al. 1995). The associated intense photon flux induces a range of photo-disintegration processes shifting the existing distribution of seed abundances to the proton rich side of the valley of stability by (γ, n) -reactions. When this process becomes less efficient because the neutron binding energy increases with neutron deficiency, the reaction flux is maintained by the (γ, p) and (γ, α) channels. After the shock front has passed the Ne/O layers, temperature and density drop exponentially and the unstable proton rich nuclei decay back to the valley of stability. In chapter 3 the p -process reaction flux will be discussed more quantitatively in terms of our present model predictions.

The description of the entire synthesis process for the p nuclei requires a comprehensive reaction network involving far more than ten thousand reactions. With very few exceptions the astrophysical reaction rates have been calculated by means of the statistical Hauser-Feshbach (HF) model, which can only be applied for nuclei with high level densities. The statistical model entries depend on free parameters for the particle potentials and level densities, as well as for the γ widths. These parameters have to be determined, tested, and improved by laboratory measurements. The HF predictions do also depend critically on the masses of the associated nuclei, which are rather well known in the case of the p process (Audi et al. 2003). A detailed description of HF techniques for determining nuclear reaction rates are given in the literature (Rauscher & Thielemann 2000, 2001, 2004). The presently available HF models describe the astrophysical reaction rates typically only within a factor of two. The specific limitations with respect to p -process analyses have been discussed by Arnould & Goriely (2003). The observed discrepancies between experimental data and theoretical HF predictions seem to be largest in the case of α capture reactions which has been interpreted as the result of the use of insufficient α potential models. We therefore will give special consideration to the impact of uncertainties in (γ, α) reactions on p -process reaction flow and p -nuclei abundance predictions.

2. EXPERIMENTAL DATA

Only a few of the required reaction rates have been investigated experimentally. While in most cases experimental and theoretical rates agree within the uncertainties due to the model parameters (Arnould & Goriely 2003), significant discrepancies have been observed in some interesting cases.

Neutron capture measurements for p -process studies are available for part of the p nuclei Bao et al. (2000), whereas methods for the determination of photodisintegration cross sections and reaction rates have been developed only recently either using inverse Compton scattered laser photons (Utsunomiya et al. 2001) or electron bremsstrahlung (Vogt et al. 2001). The latter method has been successfully applied to measure (γ, n) photodisintegration reactions for the p process including the p nuclei $^{190,192}\text{Pt}$ (Vogt et al. 2001), $^{196,198}\text{Hg}$, and the

proton magic nucleus ^{204}Pb (Sonnabend et al. 2004). Good agreement with the HF predictions has been found in all these cases. Comparable data to test the reliability of (γ, n) photodisintegration processes in the mass range below $Z = 72$ are not yet available, e.g. for nuclei near the $N = 50$ and $N = 82$ closed neutron shells.

Considerable effort has been spent on determining the rates for (γ, p) and (γ, α) reactions via measurements of the inverse capture reactions. The approach has emerged as one of the major tools for testing the reliability of the HF predictions. The (p, γ) rate for the p isotope ^{96}Ru is on average a factor two below the HF results (Bork et al. 1998). On the other hand, experimental studies for the p nucleus ^{102}Pd indicate that the reaction rate for $^{102}\text{Pd}(p, \gamma)^{103}\text{Ag}$ is significantly higher than HF predictions (Özkan et al. 2002). Recent p -nuclei related proton capture studies in the lower mass range such as $^{74,76}\text{Se}(p, \gamma)^{75,77}\text{Br}$ (Gyürky et al. 2003), or $^{92,94}\text{Mo}(p, \gamma)^{93,95}\text{Tc}$ (Sauter & Käppeler 1997) compare rather well with HF predictions. Also recent proton capture reaction studies on neutron magic nuclei with $N = 50$ such as $^{88}\text{Sr}(p, \gamma)^{89}\text{Y}$ (Galanopoulos et al. 2003) and $^{89}\text{Y}(p, \gamma)^{90}\text{Zr}$ (Tsagari et al. 2004) seem to agree well with HF calculations within the parameter space of the model. In the range $Z \geq 50$ experimental proton capture rates for p nuclei are not available except for $^{112}\text{Sn}(p, \gamma)^{113}\text{Sb}$ (Chloupek et al. 1999), which seems to be in excellent agreement with HF predictions, and for $^{116}\text{Sn}(p, \gamma)^{117}\text{Sb}$, which showed again significantly higher experimental values than predicted (Özkan et al. 2002; Rapp 2004).

Compared to neutron and proton associated capture and photodisintegration processes, larger deviations from HF predictions have been reported for α capture and photodisintegration reactions into the alpha channel. The proton and neutron binding energies for nuclei along the p -process path are typically very large, which warrants the high level density conditions required for applying the HF model. For (γ, α) reactions along the p -process path, however, the α binding energy is often low and many nuclei are even α -unbound, spontaneous α -decay being only suppressed by the respective Coulomb barriers. In these cases, where deviations from HF predictions might be anticipated, the number of experimental studies is small and limited to α capture and scattering reactions on $N = 82$ and $N = 50$ closed neutron shell nuclei along the p -process path. The measurement of the $^{144}\text{Sm}(\alpha, \gamma)^{158}\text{Gd}$ reaction ($Q = -3.721$ MeV) near the $N = 82$ closed neutron shell yielded a reaction rate (Somorjai et al. 1998) nearly one order of magnitude lower than the HF predictions (Mohr et al. 1997). The calculations are based on a wide range of α potential parameters derived from extensive ^{144}Sm α elastic scattering data. Measurements of α elastic scattering on ^{92}Mo (Fülöp et al. 2001) have been used to determine the $^{96}\text{Ru}(\gamma, \alpha)^{92}\text{Mo}$ reaction rate similar to the approach of Mohr et al. (1997). This prediction depends sensitively on the potential parameters and is considerably lower than the HF calculations (Rauscher & Thielemann 2000). Similar results have been obtained in α capture measurements on the p nuclei ^{96}Ru (Rapp et al. 2002) and ^{112}Sn (Özkan et al. 2002), where the experimen-

tal rates are also much lower than the HF predictions (Rauscher & Thielemann 2000) for the temperature range between 2.5 GK and 3.5 GK. Reasonably good agreement with theory was only found in the measurement of the (α, γ) cross section of ^{70}Ge (Fülöp et al. 1996). In addition, recent (n, α) experiments on ^{147}Sm , ^{143}Nd , and ^{95}Mo (Gledenov et al. 2000; Koehler et al. 2000; Rapp et al. 2003) have shown that present statistical models overestimate the associated α -induced astrophysical rates by more than a factor of two. In the case of ^{147}Sm the α -widths distribution of the resonances showed indications of non-statistical effects (Koehler et al. 2004).

In the following we want to study the impact of the nuclear reaction rates on the p -process yields within the framework of multi-mass zone simulations. After a short summary of the model parameters we will discuss the results of the p -process nucleosynthesis simulations. These were performed by modifying the reaction rates within the uncertainty limits of the present experimental studies and of the theoretical predictions. The impact of these modifications will be analyzed in terms of the time integrated p -process reaction flux and in terms of abundance predictions for the p nuclei. A further goal of the present work is to identify the most critical reaction rates in the mass range $A > 57$ with respect to the p abundances and to identify the reactions, which need more detailed experimental investigation.

3. MODEL PARAMETERS AND SIMULATIONS

The present nuclear reaction network comprises more than 20000 reactions connecting about 1800 nuclei from hydrogen to bismuth. We have simulated the abundance evolution of the associated isotopes in the framework of a parameterized type II SN shock front model (Rayet et al. 1995). The p process was investigated in 14 different mass layers of the Ne/O burning zone of a 25 M_{\odot} star for the temperature and density profiles proposed by Yoshida et al. (2002) (see table 1). These profiles are comparable to the ones used by (Rayet et al. 1995). It should be noted that a wide range of progenitor masses are expected to contribute to the p -process. We chose here a 25 M_{\odot} star as a representative example, in part to facilitate comparison with previous work, for example Costa et al. (2000); Woosley, Heger & Weaver (2002). Rayet et al. (1995) surveyed the type II supernova p -process for a wide range of models and find only a weak dependence of the final p -process on progenitor mass.

Fig. 2 shows the temperature and density profile of the shock front passing through three of the layers reaching peak temperatures of 2.4 GK, 2.6 GK, and 2.96 GK, respectively. Table 1 lists the mass fraction of the star enclosed by each layer M_n as well as the peak temperature and density reached in each of the layers.

The final p -process abundances depend sensitively on the choice of the initial seed abundance (Arnould & Goriely 2003). In the present approach we, therefore, kept the seed abundances fixed in order to study the sensitivity of the p abundances to nuclear reaction rates. The seed abundance distribution is determined by the s - and r -process history of the stellar material at the time of star formation, which is subsequently modified by in-situ nucleosynthesis

during the evolution of the star considered. The latter aspect is particularly important since the Ne/O layers receive an abundance contribution in the mass region $A \approx 70-90$ from the weak s process, which occurs during the preceding helium and carbon burning phases (Käppeler et al. 1994; The et al. 2000). This s -process component depends on the mass of the star but also on the neutron irradiation provided by the $^{22}\text{Ne}(\alpha, n)$ neutron source. There has been some speculation that the $^{22}\text{Ne}(\alpha, n)$ source might be more efficient than previously anticipated (Costa et al. 2000), which would cause a substantial enhancement in the abundances of the p -only nuclei ^{92}Mo and ^{96}Ru . A significantly enhanced $^{22}\text{Ne}(\alpha, n)$ reaction rate would, however, result in an enormous overproduction of s -process nuclei, in sharp conflict with the observed galactic abundance patterns (Heger et al. 2002). Also, new measurements of the $^{22}\text{Ne}(\alpha, n)$ cross section at low energies (Jaeger et al. 2001) and a detailed analysis of the $^{25}\text{Mg}(n, \gamma)^{26}\text{Mg}$ reaction channel (Koehler 2002) provide stringent limits for the uncertainty of this reaction rate (Karakas et al. 2004) and exclude the suggested enhancement factor. The seed abundances for the present study (Fig. 3) were adopted from a pre-supernova evolution model of a 25 M_{\odot} star (Rayet et al. 1995; Rayet 2002; Arnould & Goriely 2003) to facilitate comparison with previous work.

For modeling the p -process nucleosynthesis yields all n -, p -, and α -induced capture rates as well as their inverse photodisintegration rates were based on the HF predictions of the NON-SMOKER code (Rauscher & Thielemann 2000). In addition, reaction rates on light nuclei with $Z \leq 8$ were included from the work of Caughlan & Fowler (1988), Wiescher et al. (1989), Rauscher et al. (1994), and Herndl et al. (1999) to account for the impact of light particle capture reactions on the proton, neutron, and alpha budget. The abundances of the following 35 p nuclei were investigated in the calculations: ^{74}Se , ^{78}Kr , ^{84}Sr , ^{92}Mo , ^{94}Mo , ^{96}Ru , ^{98}Ru , ^{102}Pd , ^{106}Cd , ^{108}Cd , ^{112}Sn , ^{113}In , ^{114}Sn , ^{115}Sn , ^{120}Te , ^{124}Xe , ^{126}Xe , ^{130}Ba , ^{132}Ba , ^{136}Ce , ^{138}La , ^{138}Ce , ^{144}Sm , ^{152}Gd , ^{156}Dy , ^{158}Dy , ^{162}Er , ^{164}Er , ^{168}Yb , ^{174}Hf , ^{180}Ta , ^{180}W , ^{184}Os , ^{190}Pt , and ^{196}Hg . Following the method described in Rayet et al. (1995) the mass fraction $X_{i,n}$ of each p nucleus i in each p -process layer n was calculated independently for all 14 layers. The total mass m_i of nucleus i was determined by the respective contributions weighted by the mass of each zone delimited by its two neighboring p -process layers,

$$m_i = \sum_{n \geq 1}^{n=13} \frac{1}{2} (X_{i,n} + X_{i,(n-1)}) \times (M_n - M_{n-1}). \quad (1)$$

with M_n representing the mass of the star within layer n .

3.1. p -process abundances

The efficiency of a particular nucleosynthesis process in contributing to the observed solar abundance distribution can be expressed by the overproduction factor $\langle F_i \rangle$, which compares the produced abundance of a given isotope i with the observed solar abundance. For the analysis of the present calculations an overproduction factor

has been defined as

$$\langle F_i \rangle = \frac{m_i}{M_{\text{tot}} X_{i0}} \quad (2)$$

with the total mass $M_{\text{tot}} = \sum_{n>1} M_n - M_{n-1} = M_{13} - M_0$ obtained by the sum over all p -process layers. The solar abundance mass fractions X_{i0} were taken from Anders et al. (1989). The averaged overproduction factor for the 35 p -only nuclei is

$$F_0 = \sum_i \frac{\langle F_i \rangle}{35}. \quad (3)$$

The normalized overproduction factor $\langle F_i \rangle / F_0$ is by definition equal to unity when the simulated abundances match with the observed solar values (Rayet et al. 1995).

Fig. 4 shows the normalized overproduction $\langle F_i \rangle / F_0$ as a function of mass number A . Given the uncertainties of the present model and the uncertainties of the nuclear input the calculated p -abundance pattern compares reasonably well with the observed solar abundances. The comparison of the results displayed in Fig. 4 with previous work relies on an identical seed abundance distribution and on similar statistical model based reaction rates. Within the expected model specific discrepancies our calculations yield a p -nuclei abundance pattern, which is very similar to the previous results. Our prediction for ^{190}Pt disagrees with the result of Rayet et al. (1995) but is consistent with the value given by Arnould & Goriely (2003). This may reflect the use of different reaction rate compilations.

The observed abundances of the p nuclei could be reproduced in most cases within a factor of three. Particular exceptions are the notorious underproduction of $^{92,94}\text{Mo}$ and $^{96,98}\text{Ru}$ and the deficiencies of ^{113}In , ^{115}Sn , and ^{138}La . Also the much debated ^{180}Ta abundance is found in agreement with previous calculations. However, this case has been treated without distinguishing between ground and isomeric state. Accordingly, the present value represents an upper limit for the p contribution to that isotope, still compatible with the significant s -process contribution from AGB stars (Käppeler et al. 2004).

The low production of the light p nuclei $^{92,94}\text{Mo}$ and $^{96,98}\text{Ru}$ has been observed in all previous p -process studies (Rayet et al. 1995; Arnould & Goriely 2003) and remains as the main enigma in p -process simulations. Possible additional nucleosynthesis scenarios for producing these isotopes have been discussed and include a ν -induced abundance component originating from the neutrino-driven supernova shock (Hoffman et al. 1996), the production in the neutron-rich, alpha-rich freeze out near the mass cut in type II supernovae (Meyer 2003), and finally the independent production mechanism by the rp process in the outer layers of accreting neutron stars (Schatz et al. 1998; Dauphas et al. 2003). Within the framework of the p -process models possible explanations have been related to modifications in the seed abundance distribution (Costa et al. 2000; Arnould & Goriely 2003), as discussed before, or were suspected to result from the nuclear physics parameters used for calculating the associated reaction rates.

Also the underproduction of ^{113}In , ^{115}Sn , ^{138}La , ^{152}Gd , and ^{164}Er has been observed in previous calculations (Rayet et al. 1995; Arnould & Goriely 2003).

No other nucleosynthesis source has been identified for ^{113}In since it is effectively shielded from the s - and r -process path (Nemeth et al. 1994; Theis et al. 1998). For the underproduced ^{115}Sn the s process provides an additional 5% production through the sequence $^{114}\text{Cd}(n,\gamma)^{115}\text{Cd}^m(\beta^-)^{115}\text{In}^m$ feeding the $1/2^-$ isomeric state in $^{115}\text{In}^m$, which subsequently decays through a weak β^- branch to ^{115}Sn (Beer et al. 1989; Nemeth et al. 1994). More significant contributions to ^{113}In and ^{115}Sn (12% and 43%, respectively) are expected from the r process via the β -unstable isomers in ^{113}Cd and ^{115}In , which are populated in the post- r -process decay chains (Nemeth et al. 1994; Theis et al. 1998). Nevertheless, the origin of the rare In and Sn isotopes represents an unsolved puzzle.

The abundances of ^{152}Gd and of ^{164}Er , however, are understood to result mostly from s -process nucleosynthesis. In total 71% of ^{152}Gd are produced by the s -process branching at ^{151}Sm (Abbondanno et al. 2004). The here observed abundances for ^{152}Gd originate mainly at relatively cool temperatures $T_9 < 2.0$ typical for the outer p -process layers. Similarly, ^{164}Er is underproduced by the p process but more than 90% can be explained by feeding through the high temperature s -process branching via bound-state β -decay of ^{163}Dy to ^{163}Ho with the subsequent neutron capture sequence $^{163}\text{Ho}(n,\gamma)^{164}\text{Ho}(\beta^-)^{164}\text{Er}$ (Jaag & Käppeler 1996; Best et al. 2001).

The nucleus ^{138}La is systematically underproduced in all supernova based p -process models (Arnould & Goriely 2003). Alternative models related to energetic stellar particles (Hainebach et al. 1976) or neutrino interactions (Woosley et al. 1990) have been developed to explain the observed ^{138}La abundances. A detailed analysis of the ^{138}La problem has been reported by Goriely et al. (2001). In terms of nuclear reaction rates it was shown that plausible estimates for the related uncertainties can not explain the underproduction of ^{138}La . This uncertainty could be removed, however, if the theoretical production rate $^{139}\text{La}(\gamma,n)$ and the destruction rate $^{138}\text{La}(\gamma,n)$ could be replaced by experimental data.

The final p abundances depend on the p -process reaction flux and reaction branchings, which determine the feeding and depletion of the various p nuclides. In the following section we discuss the characteristic flux patterns as a function of mass layer and/or peak temperature.

3.2. p -process flux

The time integrated reaction flux per mass layer provides information about the main reaction path during the nucleosynthesis event and serves as a tool for monitoring the effects of nuclear structure parameters such as shell closure or deformation on reaction path and reaction branchings. The time integrated reaction flux corresponds to the net number of reactions between two isotopes i and j integrated over a certain period of time $\Delta t = t_1 - t_0$. This flux is defined by

$$f_{i,j} = \int_{t_0}^{t_1} \left[\frac{dY_i}{dt} \Big|_{(i \rightarrow j)} - \frac{dY_j}{dt} \Big|_{(j \rightarrow i)} \right] dt \quad (4)$$

with the isotopic abundances $Y_i = X_i/A_i$ (mass fraction divided by mass number). In the following we refer to

the time integrated reaction flux simply as reaction flux. The maximum reaction flux $f_{i,j}$ defines the main reaction path along which nucleosynthesis will take place.

The reaction flux has been calculated separately for each investigated layer and depends strongly on the respective peak temperatures. The temperature and density profiles are shown in Fig. 2. Fig. 5 shows the reaction flux integrated over a 1 s time interval covering the entire shock-driven temperature peak of $T_9=2.96$ shown in Fig. 2. During this period the seed nuclei in the range $62 < Z < 83$ are processed by (γ,n) reactions towards the neutron deficient side of stability (upper part). With increasing neutron binding energy of the reaction products (Fig. 6) the abundance distribution is driven towards lower masses by the competing (γ,α) channel. Because the neutron deficient isotopes above $N=82$ are α -unbound as shown in Fig. 7, spontaneous decay is only inhibited by the high Coulomb barriers. For neutron magic nuclei the rapid increase in neutron and α binding energy reduces the (γ,n) and (γ,α) photodisintegration rates significantly and forces the reaction flux into the (γ,p) channel along the $N=82$ closed shell nuclei towards lower masses. In particular the p -process isotope ^{144}Sm is formed by feeding through the $^{147}\text{Eu}(\gamma,p)$ and the $^{148}\text{Gd}(\gamma,\alpha)$ channels, but is depleted through $^{144}\text{Sm}(\gamma,n)$ photodisintegration.

The middle part of Fig. 5 shows the integrated reaction flux for $48 < Z < 62$. While in this mass range the overall reaction path is still driven by (γ,n) reactions towards the neutron deficient side of stability, the flux pattern is characterized by a strong (γ,p) reaction component towards stability for $N < 82$ since the rapid increase in α binding energy (Fig. 7) inhibits the (γ,α) channel. The (γ,α) processes regain a more competitive role for nuclei with $Z < 58$ and provide a strong reaction flux towards the even-even proton magic Sn isotopes with $Z=50$. The main reaction channels pass through ^{112}Sn and ^{114}Sn , which are both fed via (γ,n) and (γ,α) reactions.

The p -process flux below $Z=50$ (lower part of Fig. 5) is still characterized by (γ,α) reactions feeding the p nuclei $^{106,108}\text{Cd}$, ^{102}Pd and eventually ^{96}Ru and ^{92}Mo . At $N=50$ the (γ,α) flux is largely diminished because the increasing α binding energy efficiently reduces the (γ,α) channel. An additional strong (γ,n) and (γ,p) flux occurs towards $N=50$ closed neutron shell nuclei, which is followed by (γ,p) photodisintegration along the $N=50$ isotone chain. Compared to the integrated flux in the region $Z \geq 50$ the overall flux is significantly reduced because of the high single particle binding energies in this region near the $Z, N=50$ closed shells. The figure indicates that the abundances of the underproduced p nuclei such as ^{92}Mo and ^{96}Ru are mainly determined by the (γ,n) reaction flux feeding and the (γ,p) flux depleting these isotopes. In addition there is a significant flux through the $^{96}\text{Ru}(\gamma,\alpha)^{92}\text{Mo}$ reaction. The final abundances of the p nuclei ^{94}Mo and ^{98}Ru depend mainly on the (γ,n) rates depleting these isotopes with ^{94}Mo being mainly produced at the lower temperature mass zones. Only a few (γ,α) rates contribute to the reaction flux at $Z < 50$, mainly due to the rapid increase in α -binding energy as shown in Fig. 7.

In the mass range below the $N=50$ neutron shell the nuclei become more and more resistant against photodisintegration because of their high neutron and proton

binding energies (Figs. 6 and 8). The reaction flux is characterized by a complex pattern of single neutron, and proton capture and their inverse dissociation reactions. These processes are accompanied by (p,n) and inverse (n,p) reactions because of their typically low thresholds of $\approx 0.5 - 1.0$ MeV. The reaction path remains close to stability.

A case of p -process nucleosynthesis in a layer reaching only a peak temperature of $T_9=2.44$ is displayed in Fig. 9. For isotopes with $62 < Z < 82$, shown in the upper part of the figure, the reaction flux is dominated by (γ,n) reactions, which drive the initial seed abundance distribution towards the neutron deficient side of the line of stability. After the shock front passed, the produced radioactive isotopes decay back to the line of stability. Only minor changes are anticipated for the overall abundance distribution in this mass range. Besides the (γ,n) reactions a few (γ,α) reactions can be observed processing neutron deficient isotopes in the Hf to Pt range towards lower masses. At these temperatures the production of ^{162}Er and ^{184}Os (Fig. 10) is limited to the (γ,n) reactions along the $Z=68$ and $Z=76$ isotope chains, respectively. In the case of ^{164}Er , no feeding through $^{168}\text{Yb}(\gamma,\alpha)^{164}\text{Er}$ seems to be taking place. The p contribution to ^{152}Gd depends on the (γ,n) reactions along the $Z=64$ isotope chain, but is further depleted through $^{152}\text{Gd}(\gamma,\alpha)^{148}\text{Sm}$. The $N=82$ closed shell isotope ^{144}Sm is mainly fed by $^{148}\text{Gd}(\gamma,\alpha)^{144}\text{Sm}$ reactions.

In this mass layer the time integrated flux between the $N=82$ and $Z=50$ closed shells is again dominated by (γ,n) reactions subsequently balanced by inverse (n,γ) neutron capture reactions as shown in Fig. 9. Therefore, the abundance distribution changes only along the isotopic chain. Both (γ,p) and (γ,α) reactions are negligible. The p nuclei in this mass range are not affected by the reaction flux with two exceptions, ^{138}La and ^{138}Ce . This pattern continues also towards lower masses down to the $N=50$ neutron closed shell. The (γ,n) reaction flux associated with the $^{92,94}\text{Mo}$ and $^{96,98}\text{Ru}$ nuclei is negligible because of the high neutron binding energies. These results suggest that the p -process production of these isotopes is confined to higher temperature layers.

For nuclei below the $N=50$ closed neutron shell the reaction pattern differs distinctively from the higher mass regions. Similar to the flux at higher temperatures, photodisintegration into the neutron and proton channel and their inverse capture processes as well as (p,n) and inverse (n,p) reactions define the reaction path and determine the final abundance distribution in the mass range below $N=50$.

As shown in Figs. 5 and 9 the integrated p -process reaction flux is considerably different between high ($T_9=2.96$) and low temperature ($T_9=2.4$) layers. In particular the nucleosynthesis of higher mass p nuclei such as ^{156}Dy , ^{162}Er , ^{164}Er , ^{168}Yb , ^{174}Hf , ^{180}W , ^{184}Os , and ^{190}Pt is temperature sensitive because of the strong temperature dependence in the (γ,α) reaction rates, which determine the reaction flux pattern. The critical peak temperature for these reactions is $T_9=2.6$, where the reaction path is still largely characterized by a strong (γ,α) flux towards lower mass isotopes. Below $T_9=2.6$ the (γ,α) reaction rates are typically too weak to warrant rapid depletion of high Z isotopes. This causes an enrichment of the p nuclei through (γ,n) feeding from the initial seed

abundance distribution. For temperatures above 2.6 GK the abundances of the heavy p nuclei are reduced due to significant (γ, α) depletion, which increases exponentially with temperature.

The reaction flux depends on the initial seed abundance as well as on the reaction rates. It has been argued (Arnould & Goriely 2003) that the reaction rates have only a limited influence on the final p -process abundance distribution and in particular will not solve the mystery of the light p -nuclei abundances. In the following we seek to investigate in an independent systematic study the direct impact of p -process reaction rates.

4. THE INFLUENCE OF REACTION RATES

The influence of reaction rates on the final p -process abundance distribution was studied first by introducing global enhancement and reduction factors for different reaction channels and by probing the sensitivity of the different (γ, n) , (γ, α) , and (γ, p) photodisintegration branches. All other input parameters and conditions remain unchanged in the model. The approach of collectively changing all rates helps to identify the mass range where rates have a direct impact on the p -process flux and p -process abundance predictions. The final p -abundances are sensitive to reaction rates because they determine the balance of feeding and depletion flows for each p -nucleus. In addition, changes in reaction rates change branching ratios when several reaction channels compete, for example (γ, n) with (γ, p) in the element range up to $Z = 64$ (see Fig. 5). In addition, such branchings are sensitive to nuclear structure effects such as shell closures.

4.1. Collective change of neutron- proton- and α -rates

As a first test of the sensitivity of the p -abundance distribution the reaction rates for all neutron-induced processes and their inverse photodisintegration reactions on nuclei with $A > 57$ were enhanced or reduced by a factor of three. In each case the p abundances were calculated and the overproduction factors were compared with the results based on the standard set of HF rates used in this study (Rauscher & Thielemann 2000). Sensitivity studies for proton- and α -induced rates were performed in a similar way. Fig. 10 shows the respective overproduction factors calculated with the modified rates in comparison with the ones obtained with the standard HF rates.

The impact of the collective change of all (n, γ) and of the inverse (γ, n) rates on the p -nuclei abundances is shown in the top part of Fig. 10. One observes a correlation over the entire mass range between the rates for the neutron channel and the p -process yields. This is not too surprising because (γ, n) -reactions are active in all of the investigated layers where the p process is taking place. The overall abundances of the p nuclei change by less than a factor of two on average. Since the reaction flux below $N = 50$ is driven by capture and photodisintegration reactions the abundances of p nuclei with $A \leq 80$ correlate more strongly with changes of the reaction rate. A more pronounced correlation can also be observed for ^{162}Er , ^{164}Er , and ^{168}Yb , which are sensitive to the (γ, n) photodisintegration rates in the mass layers exposed to lower peak temperatures $2.76 \leq T_9 \leq 2.32$ as indicated for the example of ^{162}Er in Fig. 11.

The middle part of Fig. 10 displays the sensitivity of

the predictions to global changes in the proton-induced and inverse reaction rates. No impact can be observed in the mass range $A \geq 110$ despite the fact that the reaction flux pattern shows a pronounced (γ, p) flux component between $N = 50$ and $N = 82$. In our model the only exception is ^{126}Xe , which is produced by β -decay of ^{126}Ba . The final abundance depends strongly on the (γ, p) production chain of ^{126}Ba in the higher temperature mass layers. A more pronounced effect is obtained in the lower mass range $A < 110$ where the p nuclei with $Z \leq 50$ and $N \geq 50$, such as ^{92}Mo and ^{96}Ru , are mostly depleted by (γ, p) photodisintegration (Figs. 5 and 9). A reduction in rate is therefore directly correlated with an increase in abundance. The high neutron and alpha binding energies of the neutron magic nuclei with $N = 50$ terminate the (γ, n) -reaction flux at ^{92}Mo (see Figs. 6 and 7). At this point the flux continues only via the (γ, p) rate because of the relatively low proton binding energy (see Fig. 8). Hence, the ^{92}Mo abundance is strongly determined by the rate of the $^{92}\text{Mo}(\gamma, p)$ reaction. In contrast, the $^{94}\text{Mo}(\gamma, p)$ reaction has no effect on the ^{94}Mo abundance since the much lower neutron binding energy of this isotope results in a dominance of the (γ, n) channel. Similarly, ^{96}Ru and ^{98}Ru are both strongly bound against (γ, n) reactions (see Fig. 8), but ^{96}Ru has a sufficiently small proton binding energy as well to exhibit a clear sensitivity to changes of the (γ, p) rate. Therefore, the final abundances of the p nuclei ^{94}Mo and ^{98}Ru remain unaffected by changes in the (γ, p) rates. The abundances of p nuclei in the low mass range, such as ^{74}Se and ^{78}Kr correlate inversely with the strength of the proton capture reactions (chapter 4.4).

Global variation of the (α, γ) and (γ, α) rates has a strong impact on the p -nuclei abundances above $A = 140$ and $N \geq 82$ as shown in the bottom panel of Fig. 10. In this range the reaction pattern is strongly affected by (γ, α) photodisintegration reactions (Figs. 5 and 9). With increased rates the higher mass p nuclei are bypassed and the material is processed towards the lower mass p nuclei such as ^{144}Sm , ^{156}Dy and ^{162}Er . If the reaction rates are lower, processing towards these p nuclei is less efficient and causes a relative enrichment in the higher mass nuclei such as ^{174}Hf , ^{180}W , and ^{190}Pt . The abundance of ^{152}Gd remains unaffected by changes in the α capture or emission rates. In the case of ^{164}Er , variation of the (γ, α) rates leads always to a decrease in abundance. If the rate is reduced the direct feeding through $^{168}\text{Yb}(\gamma, \alpha)^{164}\text{Er}$ is suppressed, and if it is increased the abundances of higher mass feeding isotopes are reduced by faster processing towards lower mass $N = 82$ isotones. In the lower mass range the abundance of ^{96}Ru is by far the most sensitive to changes in the (γ, α) rates. Since the depletion depends significantly on the $^{96}\text{Ru}(\gamma, \alpha)$ rate, a corresponding enhancement of this rate causes a substantial reduction in the ^{96}Ru abundance. This is similar to the case of enhancing the $^{96}\text{Ru}(\gamma, p)$ depletion rate discussed above.

As pointed out before, experimental studies indicate deviations of up to one order of magnitude with respect to HF predictions for α capture and their inverse photodisintegration processes. We therefore performed a second p -process simulation with the (γ, α) rates modified by factors of 0.1 and 10, respectively, to account for a broader range of uncertainty. Fig. 12 shows that these

changes result in a similar pattern as observed in the previous study (bottom panel of Fig. 10). A significant change can only be discerned for ^{156}Dy , ^{162}Er , and to a lesser extent for ^{190}Pt . The increase with higher reaction rates is due to enhanced feeding of ^{156}Dy and ^{162}Er through (γ, α) reactions in the mass zones with lower peak temperatures (Fig. 11).

We have focused so far on global changes of reaction rates. In the following we discuss the impact of reactions feeding or depleting only the p nuclei in order to determine how critical these reactions are for the overall abundance predictions.

4.2. Impact of rates for p -nuclei reactions

Similar to the discussion before, the rates directly feeding or depleting the p nuclei were changed by factors of three to see if the calculated p -process abundances are determined by the global reaction flux or if they are associated with these specific reactions. This will have consequences for the identification of reactions to be selected for further experimental studies.

Changing the neutron capture rates and the respective photodissociation rates into the neutron channel by a factor of three produced only negligible changes in the resulting p abundances compared with the results of the global rate changes. In particular the change of (n, γ) -rates on the p nuclei showed almost no influence while the change of the (γ, n) -reactions showed mainly a slight sensitivity between $80 < A < 160$. Since (γ, n) photodisintegration processes provide the main feeding path for the transformation of the initial seed nuclei towards neutron deficient isotopes no specific outstanding reactions could be identified in this analysis. The reason is that the p -process reaction flow proceeds through neutron deficient nuclei several mass units away from stability. With increasing neutron separation energy the (γ, n) reaction rates decline rapidly and the reaction flow is carried by (γ, p) and (γ, α) channels. It is important to identify these branching points which determine the overall p -process reaction flow pattern towards lower masses. The branching points are clearly temperature dependent and differ between the different burning zones. The highest sensitivity appears to be correlated with (γ, n) reactions near the $N = 50, 82$ closed neutron shells where the (γ, n) reaction flow changes into a (γ, p) dominated reaction flow pattern. In addition, the weak sensitivity of the p abundances to the (γ, n) reactions feeding the p nuclei is not unexpected. These reactions typically occur on odd N nuclei with lower Q -values and have therefore higher rates compared to neighboring (γ, n) reactions on even N nuclei. They are therefore not expected to be particularly important bottle-necks in the p -process reaction flow.

In the case of (γ, p) dissociation reactions on p nuclei and their inverse processes, a modification of these rates has a direct impact on the abundances of p nuclei in the mass range $A < 100$. Fig. 13 compares the overproduction factors of p nuclei based on the modified rates to the ones based on standard HF rates by showing the ratio as a function of atomic mass number A . The squares (factor 1/3) and crosses (factor 3) reflect the global changes of all proton related reaction rates discussed before (see also the mid part of Fig. 10), whereas the solid and dashed lines denote the corresponding ratios obtained by chang-

ing only the (γ, p) dissociation rates on p nuclei and their inverse (p, γ) reaction rates. The results indicate that the reactions directly associated with p nuclei are the most critical ones, though in a few cases ($A = 74, 102, 106, 108$) reactions on non- p nuclei are also important (see also table 2). The figure clearly shows that the (γ, p) -rates determine significantly the p abundances of ^{74}Se , ^{78}Kr , ^{84}Sr , ^{92}Mo , and ^{96}Ru since the overabundance ratios scale inversely with the rate scaling factors. Proton capture rates have almost no influence on the p abundances, they play only a role for the light p nuclei ^{74}Se and ^{84}Sr . The comparison of the overabundance predictions based on the globally changed rates and selectively changed rates suggests that for reactions involving protons the individual feeding and depleting processes of p nuclei are significant. Fig. 13 indicates that the abundances of ^{78}Kr , ^{92}Mo , and ^{96}Ru depend sensitively on the photodisintegration of these nuclei. It has been pointed out before that particularly the $^{92}\text{Mo}(\gamma, p)^{91}\text{Nb}$ rate determines the $^{92}\text{Mo}/^{92}\text{Nb}$ abundance ratio predicted by supernova models (Dauphas et al. 2003).

Also in the case of α capture and α disintegration reactions the results indicate that the produced overabundances are closely correlated to the individual feeding and depleting reactions of the light p nuclei. Correlations in specific cases have already been found in Fig. 12 with (γ, α) reactions depleting ^{74}Se , ^{96}Ru , ^{120}Te , ^{122}Xe and (γ, α) reactions feeding ^{102}Pd , ^{106}Cd , ^{144}Sm , ^{156}Dy and ^{162}Er as discussed in the chapter 4.1.

The present simulations yield low abundances for the Mo and Ru p isotopes, in agreement with previous calculations. The difficulty in solving this problem within the astrophysical model and seed distribution discussed here comes from the fact that $^{92,94}\text{Mo}$ and $^{96,98}\text{Ru}$ make up about 43% of the total solar p nucleus abundances. Therefore, increasing their overproduction significantly requires a very efficient conversion of a significant fraction of all the heavier seed nuclei into Mo and Ru. As Fig. 11 shows, an absolute overproduction factor of the order of 10 – 90 would be needed for the Ru and Mo p isotopes to be in line with heavier p nuclei, assuming that specific isotopes are roughly produced in layers of similar mass. For comparison, conversion of the entire $Z > 42$ seed into $^{92,94}\text{Mo}$ and $^{96,98}\text{Ru}$ would be required to bring their overproduction factors up to an average of 70. Even if $^{92,94}\text{Mo}$ would be produced in separate layers without coproduction of $^{96,98}\text{Ru}$ the maximum achievable overproduction factor would only be around 110. In contrast to the earlier findings of Rayet et al. (1990) using a parametrized p -process model this would be in principle sufficient, but it is difficult to see how such a major increase in Mo and Ru production efficiency could come about. Nevertheless, to investigate this issue further, we decreased the $^{92,94}\text{Mo}(\gamma, p)$ and $^{96,98}\text{Ru}(\gamma, p)$ rates to 10% of their HF prediction. These reaction rates are the main destruction mechanism for $^{92,94}\text{Mo}$ and $^{96,98}\text{Ru}$. The resulting change in abundance is shown in Fig. 14. Only a moderate enhancement of the associated abundances is observed. Accordingly, reaction rates are not responsible for the underproduction of the light p nuclei.

4.3. Critical p -process reaction rates

The simulations discussed in the previous sections indicate that within the present model relatively few selected

reaction rates have a major impact on the final p abundances. The critical rates are typically associated with a strong feeding flux or with a particular branching in the reaction flux feeding or bypassing the p nuclei (Fig. 5). The (γ, n) reactions control the overall feeding of the p -process flux from the weak s -process seed distribution, thus affecting the final p -process abundance distribution over the entire mass range. This influence is particularly visible in the range above $N = 82$ as suggested by Fig. 10 (top panel). In the following we want to concentrate on the discussion of the (γ, p) , (n, p) , and (γ, α) branchings which divert the p -process flux towards lower masses. We identified a set of (γ, p) and (n, p) reactions and the respective inverse processes to investigate their specific impact on the simulations. Table 2 also includes those reactions in the mass range $70 < A < 78$, which seem to affect the abundances of the very light p nuclei below ^{92}Mo .

A change in the rates by a constant factor can result in opposite sensitivities as can be seen for ^{74}Se and ^{78}Kr in the middle panel of Fig. 10. For proton induced reactions and their inverse reactions the ^{78}Kr abundance depends only on the depletion reaction $^{78}\text{Kr}(\gamma, p)$ (see top part of Fig. 14), hence an increase of the proton-induced rates results always in a lower ^{78}Kr abundance. In contrast, the ^{74}Se abundance depends not only on the $^{74}\text{Se}(\gamma, p)$ rate since it is produced in the high temperature layers where the flow via $^{74}\text{Ge}(p, \gamma)^{75}\text{As}$ and $^{75}\text{As}(p, n)^{75}\text{Se}(\gamma, n)$ leads to an enhancement of the ^{74}Se abundance as these rates are increased.

The influence of the selected (γ, p) and (p, n) reactions as well as their inverse processes is demonstrated in the top panel of Fig. 15, where the abundance modifications resulting from the global change of all (γ, p) and (n, p) reaction rates and their inverse processes by a factor of three (mid panel of Fig. 10) are compared with the ones based on the change of the rates listed in Table 2. The solid and dotted lines indicate the consequences of increasing and decreasing these rates by a factor of three, respectively. Within the general uncertainties the observed abundance pattern agrees very well with the abundance pattern resulting from a global change of all rates within the same boundaries and shows that the impact of (γ, p) photodisintegration processes is confined to the p -process flux in the range $Z < 50$ with the only exception of $^{126}\text{Ba}(\gamma, p)^{125}\text{Cs}$. The impact of the (γ, p) reactions on the abundance predictions for the light p nuclei ^{92}Mo and ^{96}Ru is substantial but - within the chosen boundaries - not strong enough to explain the large under-production of these crucial p nuclei. Sensitivities to the uncertainties in the reaction rates of the (p, n) processes are mainly observed in the p -process range $N \leq 50$ where photodisintegration plays a less dominant role than in the higher mass regions.

The high seed abundances in the mass region from Hg to Pb (Fig. 3) are efficiently shifted by (γ, α) reactions towards lower masses, particularly at temperatures of $T_9 = 2.6$. This mass flow is considerably enhanced by increasing the rates of the relevant reactions listed in table 3. For example, the abundances of the p nuclei ^{156}Dy and ^{162}Er exhibit a strong sensitivity on the $^{160}\text{Er}(\gamma, \alpha)^{156}\text{Dy}$ and $^{166}\text{Yb}(\gamma, \alpha)^{162}\text{Er}$ reactions, respectively. As shown in Fig. 14, increasing and decreasing these rates by factors of three results in a correspond-

ing decrease and increase of the overproduction factors of ^{156}Dy and ^{162}Er . However, the global change of the (γ, α) rates by a factor of ten as illustrated in Fig. 12 leads to an inverse trend in the overproduction factors for ^{156}Dy and ^{162}Er , which are strongly enhanced also if the rates are increased. This behavior reflects the enhanced mass flow from the abundant seeds in the Hg to Pb region. In summary, the importance of the (γ, α) reactions calls for more systematic studies in the mass region $A \geq 140$.

Table 3 lists the (γ, α) reactions, which carry a substantial reaction flux in the p process (see Fig. 5). Again, modifying these reactions within the given uncertainty range causes significant changes in the abundances of the p nuclei. This is demonstrated in the lower panel of Fig. 15 by comparing the abundance modifications resulting from the global change of all (γ, α) reactions in the network by a factor of three (bottom panel of Fig. 10) with the ones based only on the modified rates listed in Table 3. Again, the solid and dotted lines indicate the response to an increase and the reduction of these rates by a factor of three, respectively.

The changes in p -nuclei abundances based on the modification of the selected rates in Table 3 agree well with the global change of all (γ, α) rates. The figure supports the argument that the impact of the (γ, α) photodisintegration processes is mainly visible in the higher mass p -process range above $N = 82$. This underlines the particular importance of (γ, α) rates for the mass range $N \geq 82$ except for the case of the light p nuclei ^{96}Ru and ^{74}Se , where the predicted abundance is correlated with the depletion via $^{96}\text{Ru}(\gamma, \alpha)^{92}\text{Mo}$ and $^{74}\text{Se}(\gamma, \alpha)^{70}\text{Ge}$ respectively, as indicated in Fig. 5.

The analysis of the abundances for p nuclei with $N \geq 82$ indicates that the low abundances of the p nuclei ^{156}Dy , ^{162}Er , and ^{190}Pt might be due to the (γ, α) rates in that mass range, while p nuclei such as ^{152}Gd , ^{158}Dy , and ^{164}Er depend more on the strength of the particular (γ, n) feeding from the seed abundance distribution.

The results shown in Fig. 15 suggest that comparably few rates involving charged particles have a direct impact on the abundances of the p nuclei. These critical rates, which are summarized in Tables 2 and 3, carry most of the charged particle related uncertainties for simulations within the discussed p -process model frame. Since all of these rates are presently based on global HF calculations (Rauscher & Thielemann 2000, 2001, 2004), experimental confirmation is necessary for reducing the inherent nuclear model uncertainties. This serves not only the purpose of obtaining better data, but since p -process abundances are sensitive to changes in these specific rates, a better knowledge of those rates will help to improve the fine-tuning for modeling of the supernova shock front traversing the O-Ne shell of the pre-supernova star.

Our list of potentially important reactions largely differs from the one given by Rauscher (2006). This is not surprising because the latter work identifies reaction flow branchings in a more simplified approach and does not follow the hydrodynamic evolution of different p -process layers. In addition, we have not limited our analysis to branchings, and we have also included other types of reactions such as (n, p) or (p, n) .

There are experimental data for some of the listed (p, n)

reactions. Fig. 16 shows the experimental data for the $^{75}\text{As}(p,n)$ and the $^{85}\text{Rb}(p,n)$ reaction in comparison with Hauser Feshbach predictions. Only three data points have been determined for $^{75}\text{As}(p,n)$ in the energy range from 3 to 5 MeV (Kailas et al. 1979). The experimental results are in excellent agreement with the statistical Hauser Feshbach predictions (Rauscher & Thielemann 2001). On the other hand, the $^{75}\text{As}(p,n)$ cross sections obtained by a measurement of $^{75}\text{As}(p,xn)$ reactions in the energy range of 3 - 45 MeV (Mushtaquet et al. 1988) show significant discrepancies to the model predictions for the astrophysical low energy range. Experimental cross section data for the $^{85}\text{Rb}(p,n)$ reaction are available for a wide energy range from 3 MeV up to 100 MeV (Kastleier et al. 2002). The experimental results are on average lower than the Hauser Feshbach predictions (Rauscher & Thielemann 2001); on the other side, the data are handicapped by huge experimental uncertainties. In both cases independent experimental verification of the cross sections for the astrophysical energy range is desirable.

Different experimental techniques will be necessary for a complete study of these critical reactions. As mentioned before, in previous work the experimental effort concentrated on the study of capture reactions using the activation technique and in a few cases on direct photodisintegration studies with photon beams. The activation technique for capture reactions on stable nuclei is limited to cases where the final reaction products are characterized by specific γ -radiation signatures. This is necessary for uniquely identifying the reaction products and separating them from the large background activity originating from target impurities. This technique for example can be applied for the measurement of $^{75}\text{As}(p,n)^{75}\text{Se}$, $^{106}\text{Cd}(\alpha, \gamma)^{110}\text{Sn}$, or $^{196}\text{Hg}(\alpha, \gamma)^{200}\text{Pb}$, as well as a larger set of (n, γ) cross sections.

If the characteristic activity is masked by background or if the reaction product lacks characteristic activity, alternative detection methods can be envisioned through AMS methods where the reaction products are chemically separated from the activated target and analyzed through high resolution accelerator mass spectroscopy. This approach has been successfully applied in the study of the $^{62}\text{Ni}(n, \gamma)^{63}\text{Ni}$ s -process reaction (Nassar et al. 2005). Possible examples for applying this specific technique are the reactions $^{72}\text{Ge}(p, \gamma)^{73}\text{As}$, or for the higher mass range $^{156}\text{Dy}(\alpha, \gamma)^{160}\text{Er}$ or $^{190}\text{Pt}(\alpha, \gamma)^{194}\text{Hg}$, which are characterized by such a low Q_β value that a measurement of the decay activity is difficult.

Inverse photodisintegration measurements have also been developed as a powerful experimental tool (Utsumomiya et al. 2001; Vogt et al. 2001). The increasing availability of high energy photon beams at the HIGS facility at TUNL (<http://higs.tunl.duke.edu/>) or at the ELBE facility of the Forschungszentrum Rossendorf

(<http://www.fz-rossendorf.de/pls/rois/Cms?pNid=144>) opens new opportunities for targeting reactions such as $^{74}\text{Se}(\gamma, p)^{73}\text{As}$, $^{92}\text{Mo}(\gamma, p)^{91}\text{Nb}$, and $^{96}\text{Ru}(\gamma, p)^{95}\text{Tc}$, which directly affect the light p -nuclei abundances. Again, the reaction product can be detected by measuring the characteristic activity. If the latter is masked by background or falls below present detection limits alternative analytical methods such as the AMS approach

can be applied.

Many of the reactions listed in Tables 2 and 3, however, are photodisintegration processes on radioactive nuclei leading to radioactive nuclei; reactions with significant impact on flux and abundances are $^{110}\text{Sn}(\gamma, p)^{109}\text{In}$, $^{126}\text{Ba}(\gamma, p)^{125}\text{Cs}$, or in the range $N \geq 82$, for example $^{152}\text{Dy}(\gamma, \alpha)^{148}\text{Gd}$, $^{160}\text{Yb}(\gamma, \alpha)^{156}\text{Er}$. Such reactions can be approached by Coulomb dissociation techniques with radioactive beams. In the specific p -process cases listed here heavy ion radioactive beams have to be developed in the energy range of 2-12 MeV/amu depending on the associated Q -values. Coulomb dissociation techniques are typically applied for studies with light radioactive particles, which are produced through beam fragmentation reactions. Such cases are suited for facilities such as the NSCL at MSU, at RIKEN, and at GSI where heavy neutron deficient radioactive particles can be produced by spallation or heavy ion evaporation reactions at inverse kinematics.

5. SUMMARY

We have investigated the reaction flux patterns of the p process within the framework of a multi-mass zone type II supernova shock front model. Particular attention was paid to the influence of p -process reaction rates within the uncertainty limits of the theoretical Hauser-Feshbach model. The predicted p abundances are similar to the ones observed by previous work in this field. It could be shown that the endemic underproduction of the light p nuclei $^{92,94}\text{Mo}$ and $^{96,98}\text{Ru}$ are not due to the uncertainties in the thermonuclear reaction rates and must be traced back to other reasons. Possible neutron poison reactions in core helium burning and secondary neutron sources during core carbon burning could modify significantly the weak s -process seed abundance distribution for the p -process. This was not considered in the present paper. It should be addressed in future studies to investigate systematically the s -process related uncertainties for p -process simulations.

Since (γ, n) reactions control the overall feeding of the p -process flux, the corresponding reaction rates affect the final p -process abundance distribution over the entire mass range. This influence is particularly visible in the range above $N = 82$. On the other hand we found that the impact of (γ, p) and (γ, α) reactions is limited to specific mass regions. Changes in the (γ, p) reactions translate to direct modifications of the p -process abundances in the lower mass range with $Z \leq 50$, but similar correlations were not observed in the higher mass range. In contrast, variations in the (γ, α) reaction rates impact the abundance predictions in the higher mass range above $N = 82$, while only small effects can be observed at lower masses. The overall impact of reaction rates seems not as dramatic as for other processes, the here discussed modifications of the rates translated in general to a change in the absolute abundances of a factor two to three. This will directly affect the overproduction factors displayed in Fig. 4. Improved data are necessary since a reduction of the associated uncertainty will help to identify more clearly other uncertainty factors in the present simulation. This includes the uncertainties resulting from the initial seed distribution or uncertainties yielding from insufficient model descriptions of the p -process scenario.

Past experiments have confirmed that theoretically predicted p -process reaction rates agree within a factor of two with experimentally determined proton and neutron capture and the respective photodisintegration data. For the corresponding α rates considerably larger differences of up to a factor of ten were reported. More experimental work is necessary to test the validity of the α potentials used in the model calculations. It is also necessary to expand the experimental work towards p -process reaction studies on neutron deficient nuclei to verify the reliability of the theoretical predictions for reactions involving radioactive nuclei.

6. ACKNOWLEDGEMENT

REFERENCES

- Abbondanno, U. et al. 2004, *Phys. Rev. Lett.* 93, 161103
- Anders, E., & Grevesse, N. 1989, *Geochim. Cosmochim. Acta* 53, 197
- Arnould, M., & Goriely, S. 2003, *Phys. Rep.* 384, 1
- Audi, G., Wapstra, A. H., & Thibault, C. 2003, *Nucl. Phys.*, A729, 337
- Baleisis, A., and Arnett, W. D. 2001, *Nucl. Phys. A* 688, 185c
- Bao, Z. Y., Beer, H., Käppeler, F., Voss, F., Wisshak, K., & Rauscher, T. 2000, *At. Data Nucl. Data Tables*, 76, 70
- Beer, H., Walter, G., & Käppeler, F. 1989, *A&A*, 211, 245
- Best, J., Stoll, H., Arlandini, C., Käppeler, F., Wisshak, K., Mengoni, A., Reffo, G., & Rauscher, T. 2001, *Phys. Rev.*, C64, 015801
- Bork, J., Schatz, H., Käppeler, F., & Rauscher, T. 1998, *Phys. Rev. C*, 58, 524
- Caughlan, G. & Fowler, W. A. 1988, *At. Data Nucl. Data Tables*, 40, 283
- Chloupek, F. R., et al. 1999, *Nucl. Phys.*, A 652, 391
- Costa, V., Rayet, M., Zappala, R. A., & Arnould, M. 2000, *A&A*, 358, L67
- Dauphas, N., Rauscher, T., Marty, B., & Reisberg, L. 2003, *Nucl. Phys.*, A719, 287c
- Fujimoto, S., Hashimoto, M., Koike, O., Arai, K., & Matsuba, R. 2003, *ApJ*, 585, 418
- Fülöp, Zs., Kiss, A. Z., Somorjai, E., Rolfs, C. E., Trautvetter, H.-P., Rauscher, T., & Oberhummer, H. 1996, *Z. Phys.*, A 355, 203
- Fülöp, Zs., et al. 2001, *Phys. Rev. C*, 64, 065805
- Galanopoulos, et al. 2003, *Phys. Rev. C*, 67, 015801
- Gledenov, Y., Koehler, P. E., Andrzejewski, J., Guber, K. H., & Rauscher, T. 2000, *Phys. Rev. C*, 62, 04280(R)
- Goriely, S., Arnould, M., Borzov, I., & Rayet, M. 2001, *A&A*, 375, L35
- Gyürky, Gy., et al. 2003, *Phys. Rev. C*, 68, 055803
- Hainebach, K. L., Schramm, D. N., & Blake, J. B. 1976, *ApJ*, 205, 920
- Hayakawa, T., Iwamoto, N., Shizuma, T., Kajino, T., Umeda, H., & Nomoto, K. 2004, *Phys. Rev. Lett.*, 93, 161102
- Heger, A., Woosley, S. E., Rauscher, T., Hoffman, R. D., & Boyes, M. M. 2002, *New Astron. Rev.*, 46, 4563
- Hernndl, H., Hofinger, R., Jank, J., Oberhummer, H., Görres, J., Wiescher, M., Thielemann, F.-K., & Brown, B. A. 1999, *Phys. Rev. C*, 60, 064614
- Hoffman, R. D., Woosley, S. E., Fuller, G. M., & Meyer, B. S. 1996, *ApJ*, 460, 478
- Howard, W. M., Meyer, B. S., & Woosley, S. E. 1991, *ApJ*, 373, L5
- Jaag, S., & Käppeler, F. 1996, *ApJ*, 464, 874
- Jaeger, M., Kunz, R., Mayer, A., Hammer, J. W., Staudt, G., Kratz, K.-L., & Pfeiffer, B. 2001, *Phys. Rev. Lett.*, 87, 202501
- Jordan, G. C., & Meyer, B. S. 2004, *ApJ*, 617, 617
- Kailas, S., Metha, M. K., Gupta, S. K., Viyogi, Y. P., & Ganguly, N. K. 1979, *Phys. Rev. C*, 20, 1272
- Käppeler, F., Beer, H., & Wisshak, K. 1989, *Rep. Prog. Phys.*, 52, 945
- Käppeler, F., et al. 1994, *ApJ*, 437, 396
- Käppeler, F. et al. 2004, *Phys. Rev. C*, 69, 055802
- Karakas, A., Lugaro, M., Ugalde, C., & Wiescher, M. 2004, *Mem. S. A. It.*, 73, 23
- Kastleier, S., Qaim, S. M., Nortier, F. M., Blessing, G., Van der Walt, T. N., & Coenen, H. H. 2002, *Applied Radiation and Isotopes* 56, 685
- Koehler, P. E., Gledenov, Y., Andrzejewski, J., Raman, S., & Rauscher, T. 2000, *Nucl. Phys. A*, 688, 86c
- Koehler, P. E. 2002, *Phys. Rev. C*, 66, 055805
- Koehler, P. E., Gledenov, Y., Rauscher, T., & Fröhlich, C. 2004, *Phys. Rev. C*, 69, 015803
- Lambert, D. 1992, *A&A Rev.*, 3, 201
- Meyer, B. S. 1994, *Ann. Rev. A&A*, 32, 153
- Meyer, B. S. 2003, *Nucl. Phys. A*, 719, 13c
- Mohr, P., Rauscher, T., Oberhummer, H., Maáté, Z., Fülöp, Zs., Somorjai, E., Jaeger, M., & Staudt, G. 1997, *Phys. Rev. C*, 55, 1523
- Mushtaq, A., Qaim, S. M., & Stoecklin, G. 1988, *Applied Radiation and Isotopes*, 39, 1085
- Nassar, H., et al. 2005, *Phys. Rev. Lett.*, in press
- Nemeth, Zs., Käppeler, F., Theis, C., Belgya, T., & Yates, S. W. 1994, *ApJ*, 426, 357
- Özkan, N., et al. 2002, *Nucl. Phys. A*, 710, 469
- Rapp, W., Heil, M., Hentschel, D., Käppeler, F., Reifarth, R., Brede, H. J., Klein, H., & Rauscher, T. 2002, *Phys. Rev. C*, 66, 015803
- Rapp, W., Koehler, P. E., Käppeler, F., & Raman S. 2003, *Phys. Rev. C*, 68, 015802
- Rapp, W. 2004, Report FZKA-6407, Forschungszentrum Karlsruhe.
- Rauscher, T., Applegate, J. H., Cowan, J. J., Thielemann, F.-K., & Wiescher, M. 1994, *ApJ*, 429, 499
- Rauscher, T., & Thielemann, F.-K. 2000, *At. Data Nucl. Data Tables*, 75, 1
- Rauscher, T., & Thielemann, F.-K. 2001, *Atomic Data Nuclear Data Tables*, 79, 47
- Rauscher, T., Heger, A., Hoffman, R. D., & Woosley, S. E. 2002, *ApJ*, 576, 323
- Rauscher T., & Thielemann, F.-K. 2004, *At. Data Nucl. Data Tables*, 88, 1
- Rauscher T. 2006, *Phys. Rev. C*, 73, 015804
- Rayet, M. 2002, private communication
- Rayet, M., Prantzos, N., & Arnould, M. 1990, *A&A*, 227, 271
- Rayet, M., Arnould, M., Hashimoto, M., Prantzos, N., & Nomoto, K. 1995, *A&A*, 298, 517
- Sauter, T., & Käppeler, F. 1997, *Phys. Rev. C*, 55, 3127
- Schatz, H. et al. 1998, *Phys. Rep.*, 294, 167
- Somorjai, E. et al. 1998, *A&A*, 333, 1112
- Sonnabend, K., Vogt, K., Galaviz, D., Müller, S., & Zilges, A. 2004, *Phys. Rev. C*, 70, 035802
- The, L.-S., El Eid, M. F., Meyer, B. S. 2000, *ApJ*, 533, 998
- Theis, C., Käppeler, F., Wisshak, K., & Voss, F. 1998, *ApJ*, 500, 1039
- Tsagari, P., Kokkoris, M., Skreti, E., Karydas, A. G., Harissopulos, S., Paradellis, T., & Demetriou, P. 2004, *Phys. Rev. C*, 70, 015802
- Utsunomiya, H., Yonezawa, Y., Akimune, H., Yamagata, T., Ohta, M., Toyokawa, H., Ohgaki, H., & Sumiyoshi, K. 2001, *Nucl. Phys. A* 688, 340c
- Vogt, K. et al. 2001, *Phys. Rev. C*, 63, 055802

Wiescher, M., Görres, J., Graff, S., Buchmann, L., & Thielemann, F.-K. 1989, *ApJ*, 343, 352
Woosley, S. E., Heger, A. & Weaver, T. A. 2002, *Rev. Mod. Phys.* 74, 1015
Woosley, S. E., Hartmann, D. H., Hoffman, R. D., & Haxton, W. C. 1990, *ApJ*, 356, 272

Woosley, S. E., & Howard, W. M. 1978, *ApJS*, 36, 285
Yoshida, T., & Hashimoto, M. 2002, private communication

TABLE 1
 MASS COORDINATE, MAXIMUM TEMPERATURE AND MAXIMUM DENSITY IN THE INVESTIGATED p -PROCESS LAYERS.

layer No.	mass inside the shell (M_{\odot})	maximum temperature (T_{g})	maximum density (10^5 g/cm^3)
1	1.9336	3.45	7.85
2	1.9658	3.11	6.64
3	2.0085	2.96	5.68
4	2.0508	2.76	4.82
5	2.1037	2.60	4.07
6	2.1564	2.44	3.56
7	2.2090	2.32	3.16
8	2.2614	2.21	2.80
9	2.3136	2.12	2.54
10	2.3655	2.04	2.30
11	2.4171	1.97	2.11
12	2.4684	1.91	1.94
13	2.5249	1.84	1.75
14	2.5825	1.79	1.68

TABLE 2

SELECTED (γ, p) OR (n, p) REACTIONS THAT TOGETHER WITH THEIR RESPECTIVE INVERSE REACTIONS WERE FOUND TO EXHIBIT THE STRONGEST INFLUENCE ON THE FINAL p ABUNDANCES. THEIR IMPACT IS ILLUSTRATED IN THE TOP PANEL OF FIG. 15. PARTICULARLY IMPORTANT RATES ARE MARKED WITH *).

$^{126}\text{Ba}(\gamma, p)^{125}\text{Cs}^*$	$^{92}\text{Mo}(\gamma, p)^{91}\text{Nb}^*$	$^{75}\text{Se}(n, p)^{75}\text{As}^*$
$^{110}\text{Sn}(\gamma, p)^{109}\text{In}^*$	$^{86}\text{Rb}(n, p)^{86}\text{Kr}^*$	$^{74}\text{Se}(\gamma, p)^{73}\text{As}^*$
$^{106}\text{Cd}(\gamma, p)^{105}\text{Ag}$	$^{85}\text{Sr}(n, p)^{85}\text{Rb}^*$	$^{76}\text{As}(n, p)^{76}\text{Ge}^*$
$^{104}\text{Cd}(\gamma, p)^{103}\text{Ag}$	$^{84}\text{Sr}(\gamma, p)^{83}\text{Rb}^*$	$^{75}\text{As}(\gamma, p)^{74}\text{Ge}$
$^{100}\text{Pd}(\gamma, p)^{99}\text{Rh}$	$^{78}\text{Kr}(\gamma, p)^{77}\text{Br}^*$	$^{73}\text{As}(\gamma, p)^{72}\text{Ge}^*$
$^{96}\text{Ru}(\gamma, p)^{95}\text{Tc}^*$	$^{77}\text{Se}(n, p)^{77}\text{As}$	$^{71}\text{Ge}(n, p)^{71}\text{Ga}$

TABLE 3

SELECTED (γ, α) REACTION CHAINS, WHICH WERE FOUND TO EXHIBIT THE STRONGEST INFLUENCE ON THE FINAL p ABUNDANCES. THEIR IMPACT IS ILLUSTRATED IN THE BOTTOM PANEL OF FIG. 15. PARTICULARLY IMPORTANT RATES ARE MARKED WITH *).

$^{74}\text{Se}(\gamma, \alpha)^{70}\text{Ge}^*$	$^{196}\text{Pb}(\gamma, \alpha)^{192}\text{Hg}^*$
$^{96}\text{Ru}(\gamma, \alpha)^{92}\text{Mo}^*$	$^{191}\text{Hg}(2\gamma, 2\alpha)^{183}\text{Os}$
$^{106}\text{Cd}(\gamma, \alpha)^{102}\text{Pd}$	$^{190}\text{Hg}(3\gamma, 3\alpha)^{178}\text{W}^*$
$^{110}\text{Sn}(\gamma, \alpha)^{106}\text{Cd}^*$	$^{189}\text{Hg}(3\gamma, 3\alpha)^{177}\text{W}$
$^{120}\text{Te}(\gamma, \alpha)^{116}\text{Sn}^*$	$^{188}\text{Hg}(5\gamma, 5\alpha)^{168}\text{Yb}^*$
$^{122}\text{Xe}(\gamma, \alpha)^{118}\text{Te}$	$^{183}\text{Pt}(3\gamma, 3\alpha)^{171}\text{Hf}$
$^{128}\text{Ba}(\gamma, \alpha)^{124}\text{Xe}^*$	$^{178}\text{Os}(4\gamma, 4\alpha)^{162}\text{Er}^*$
	$^{177}\text{Os}(3\gamma, 3\alpha)^{165}\text{Yb}$
	$^{176}\text{Os}(5\gamma, 5\alpha)^{156}\text{Dy}^*$
	$^{167}\text{Hf}(\gamma, \alpha)^{163}\text{Yb}$
	$^{166}\text{Hf}(5\gamma, 5\alpha)^{146}\text{Sm}^*$
	$^{156}\text{Er}(3\gamma, 3\alpha)^{144}\text{Sm}^*$

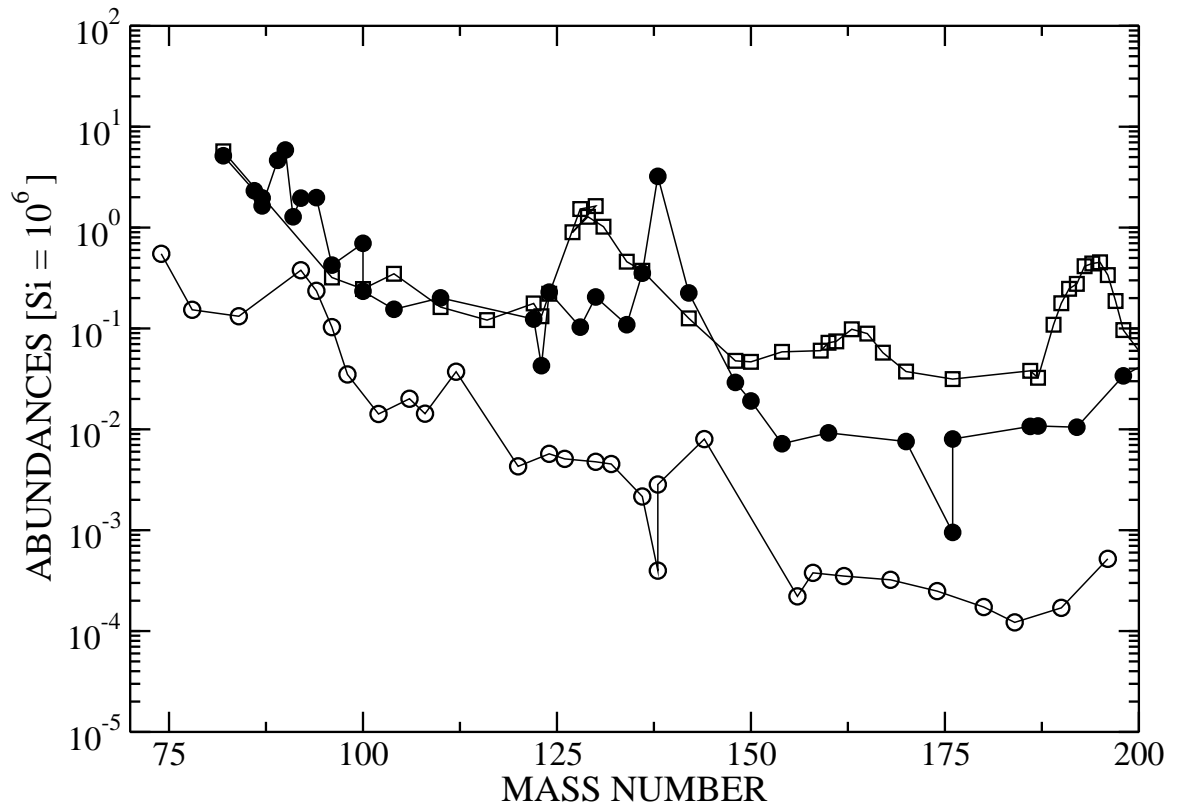


FIG. 1.— Abundance distribution of those heavy isotopes, which can be entirely ascribed to *s* process (full circles), *r* process (open squares), and *p* process (open circles) nucleosynthesis.

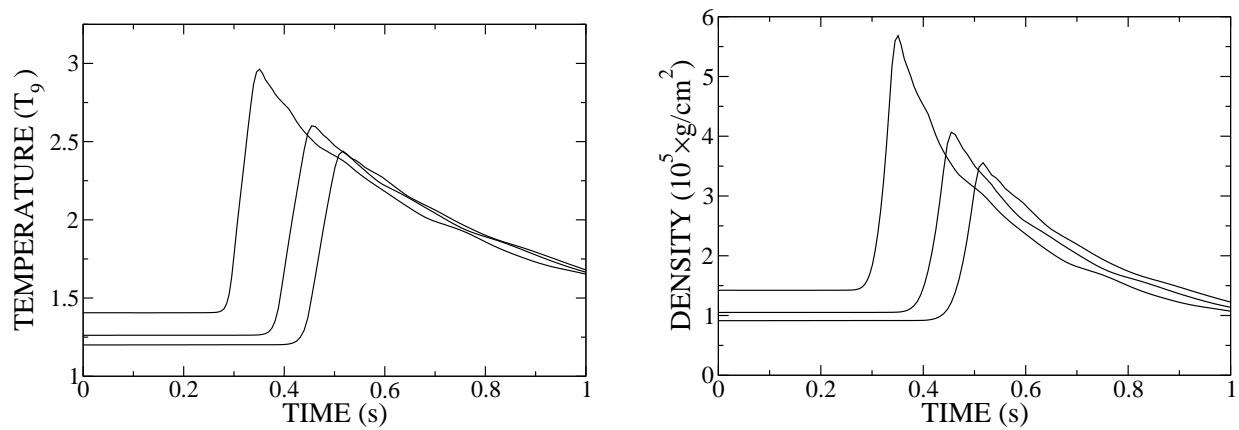


FIG. 2.— Temperature and density profiles of the supernova shock front traversing the Ne/O layer of the pre-supernova star.

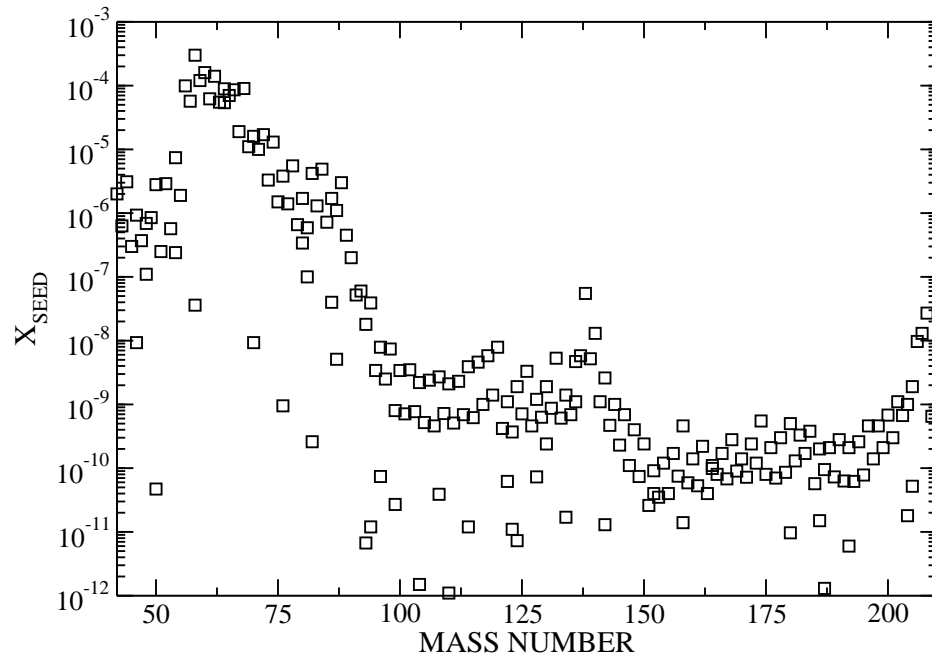


FIG. 3.— Adopted seed abundance distribution for the p -process simulations.

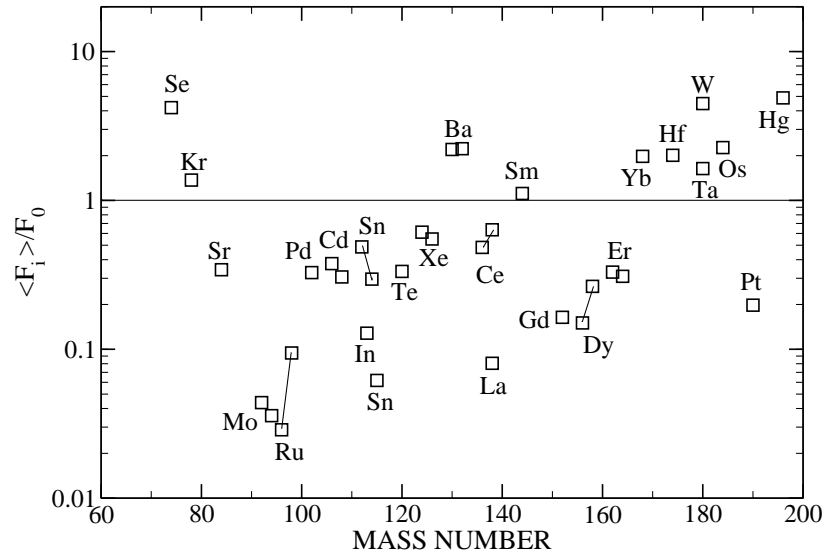


FIG. 4.— Averaged normalized overproduction factor for the proton rich p nuclei from network calculation with standard reaction rates (see text).

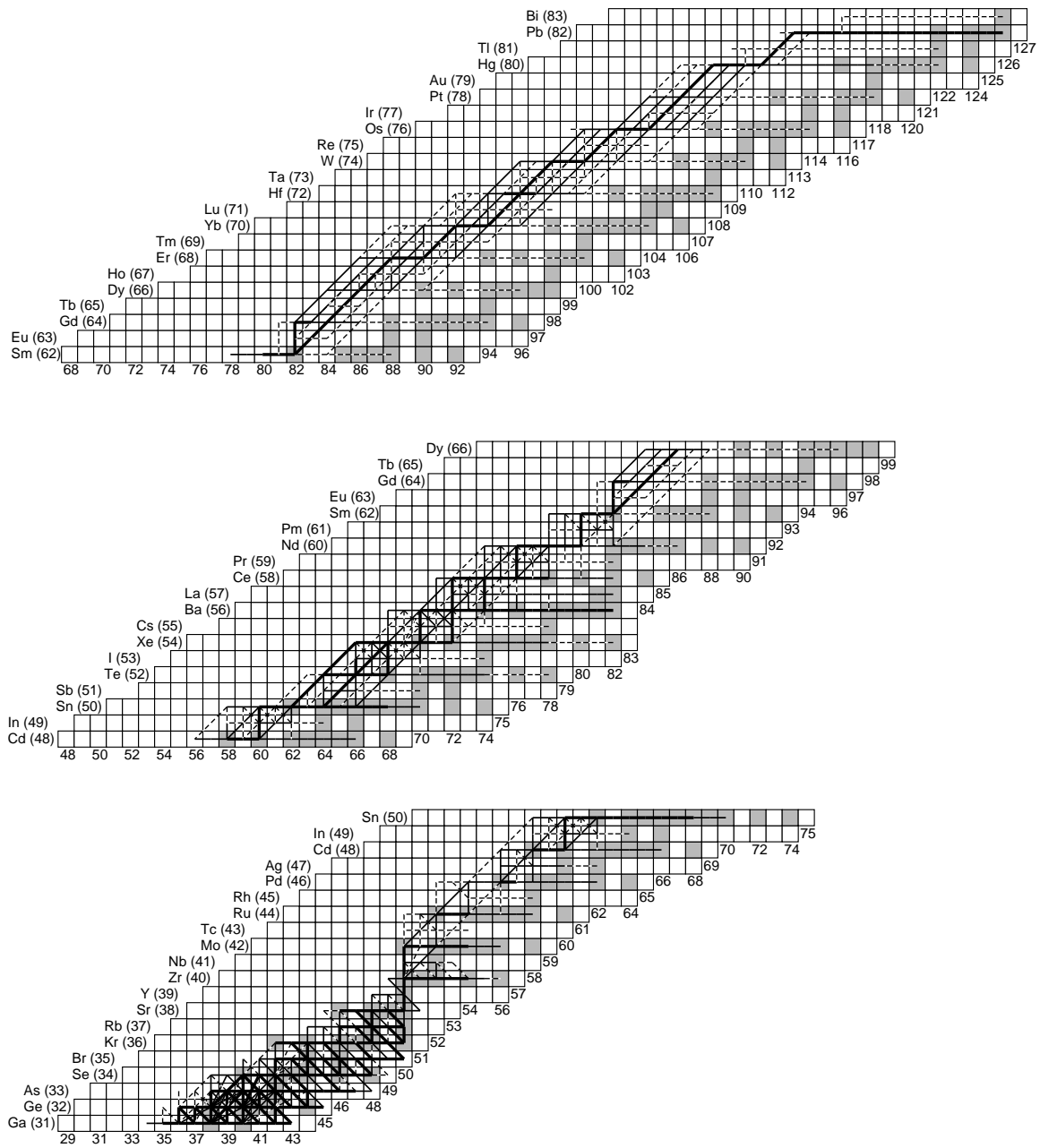


FIG. 5.— Integrated reaction flux during the first second of a type II supernova explosion in the Ne/O layer with a maximal temperature of $T_9=2.96$. The reaction flux is indicated by the line thickness (thick solid line $>10^{-10}$, solid line $>10^{-11}$, dashed line $>10^{-12}$).

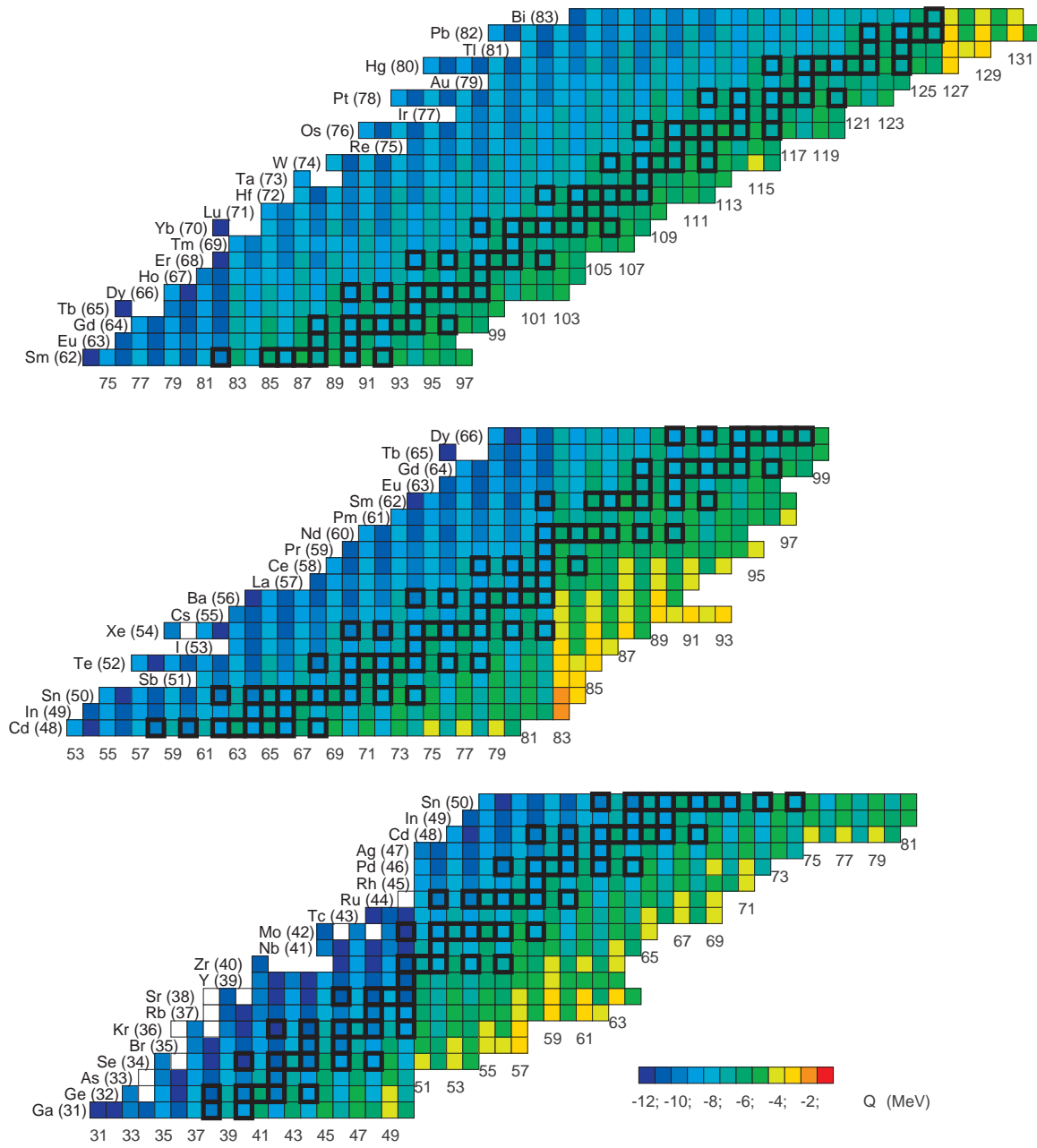


FIG. 6.— Q-values for (γ, n) reactions based on experimental mass data (Audi et al. 2003).

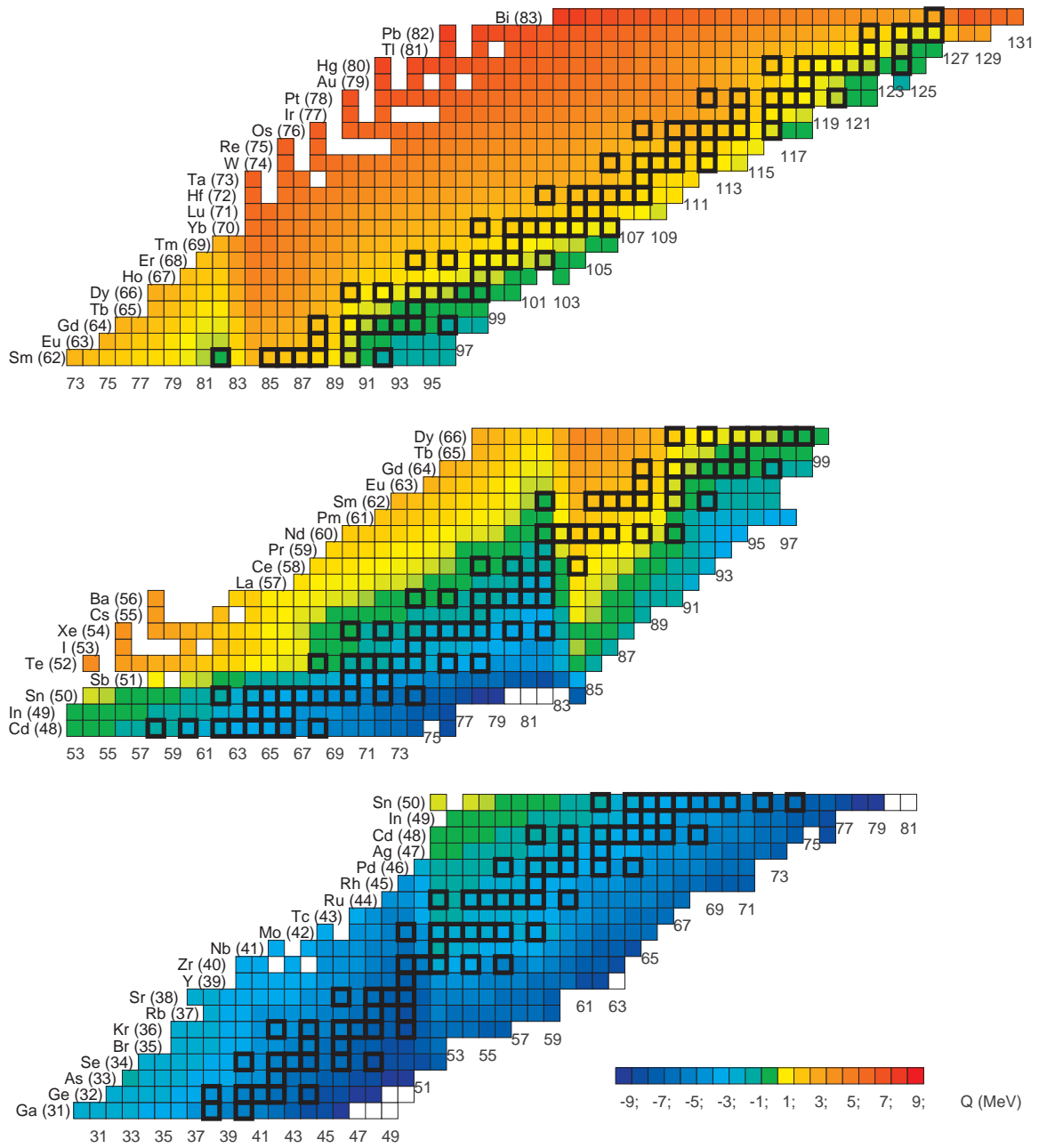


FIG. 7.— Q -values for (γ, α) reactions based on experimental mass data (Audi et al. 2003).

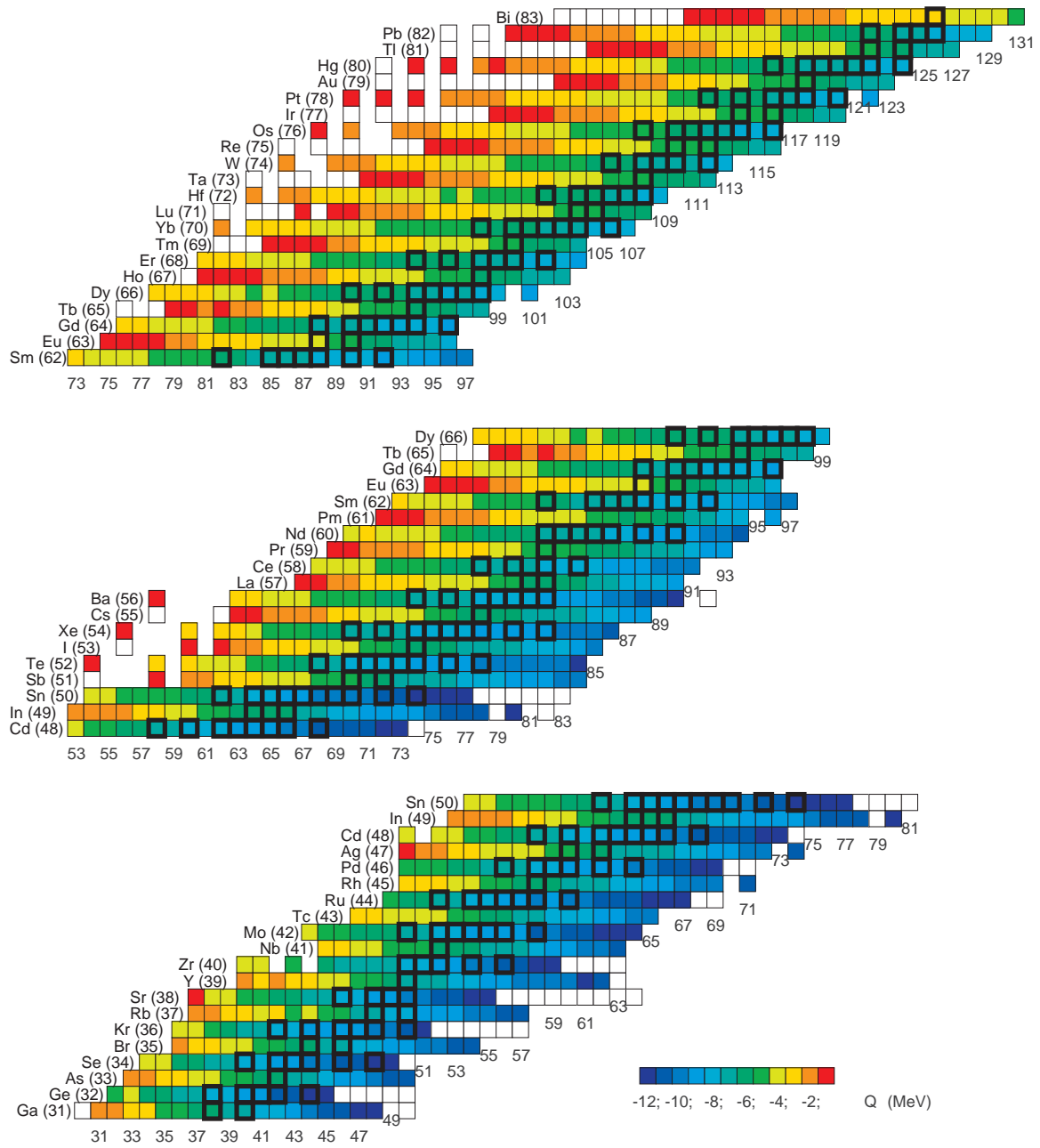


FIG. 8.— Q -values for (γ, p) reactions based on experimental mass data (Audi et al. 2003).

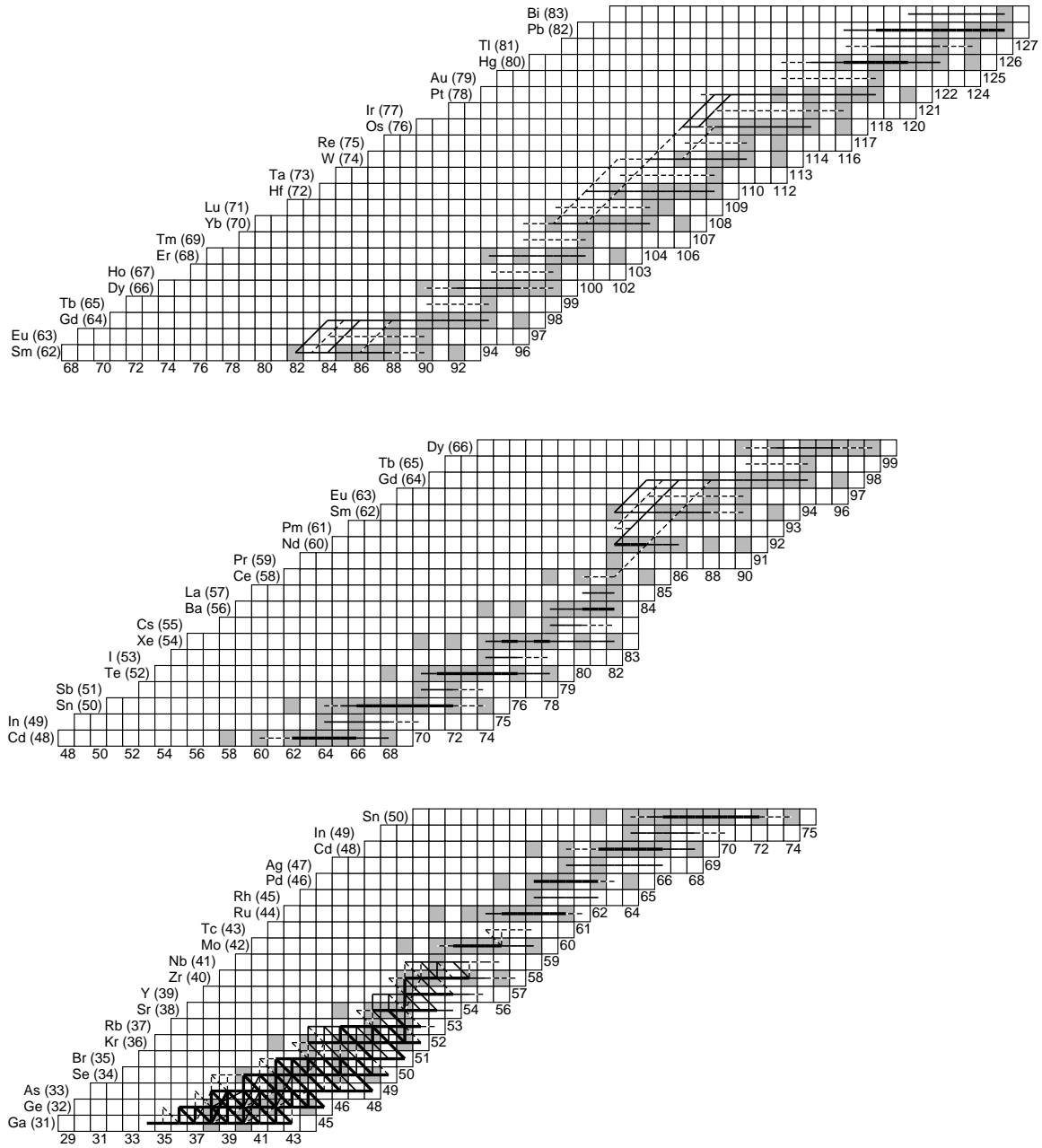


FIG. 9.— The integrated reaction flux during the first second of a type II supernova explosion in the Ne/O layer with a maximal temperature of $T_9=2.44$. The reaction flux is indicated by the line thickness (thick solid line $>10^{-11}$, solid line $>10^{-12}$, dashed line $>10^{-13}$).

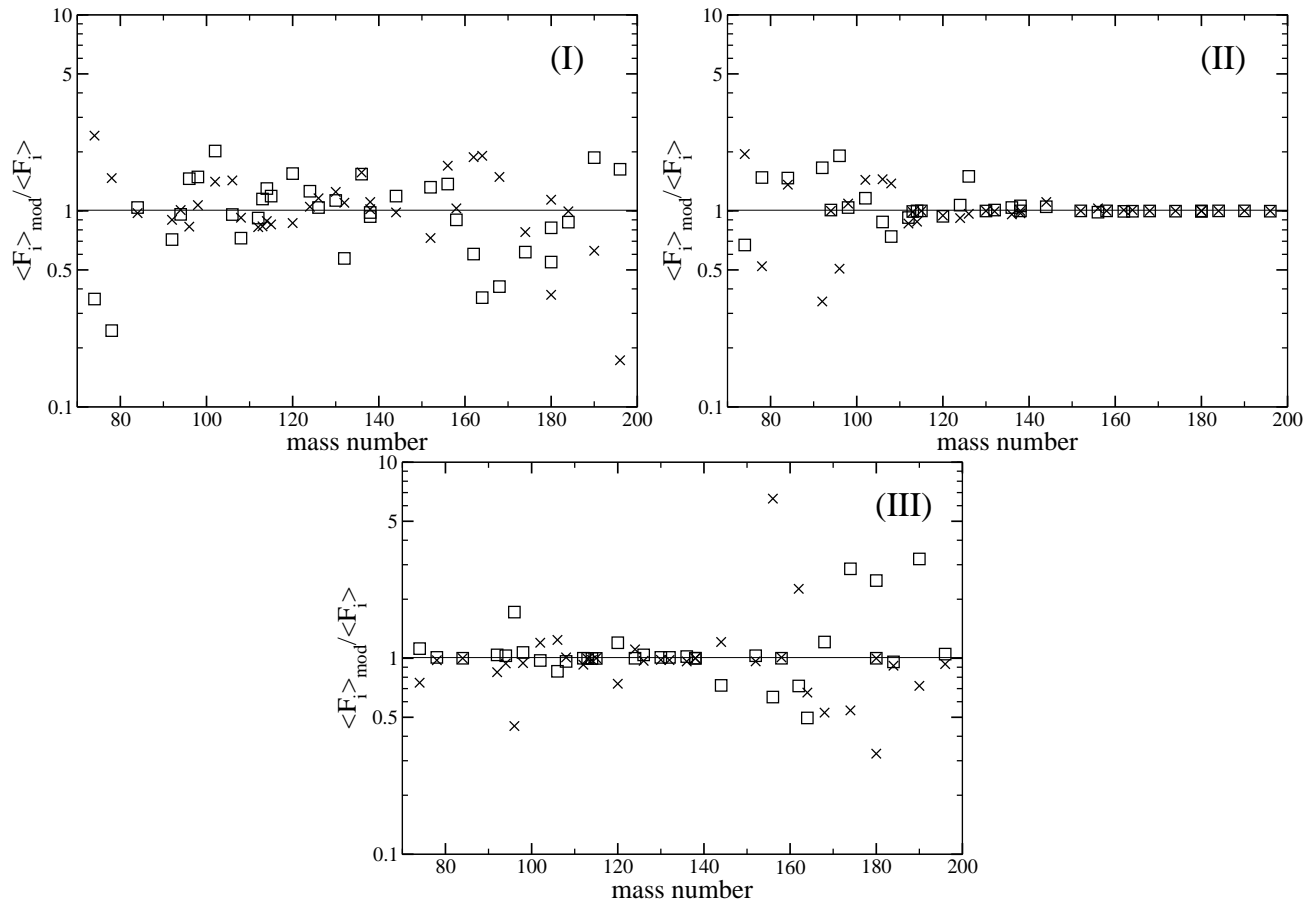


FIG. 10.— Ratio of p abundances calculated with modified rates and the presently accepted HF-rates for all n-induced (top), p-induced (middle), and α -induced reactions (bottom) and their inverse processes. Squares and crosses denote results obtained with three times smaller and larger rates, respectively.

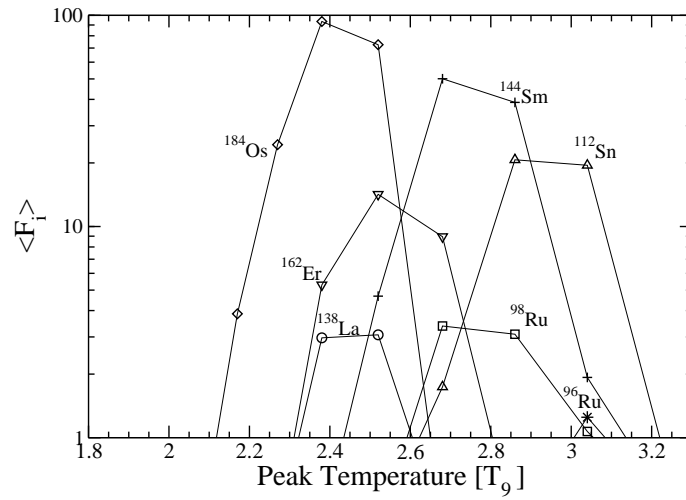


FIG. 11.— Overproduction factors for selected p nuclei (^{96}Ru , ^{98}Ru , ^{112}Sn , ^{138}La , ^{144}Sm , ^{162}Er and ^{184}Os) as a function of temperature indicating the production efficiency in the different p -process zones.

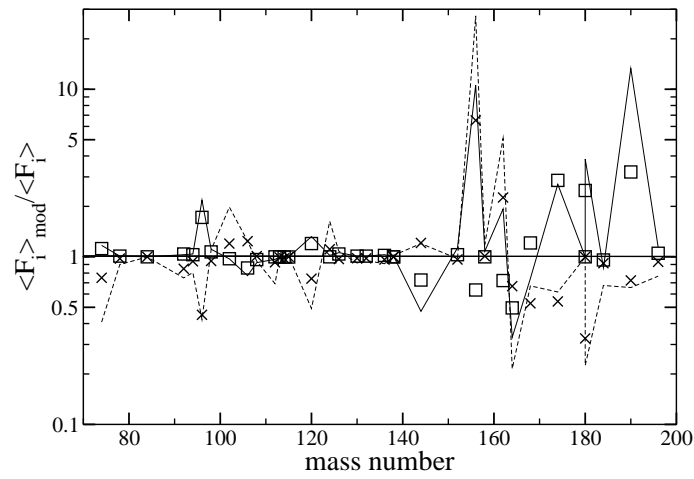


FIG. 12.— Same as bottom panel of Fig. 10, but with the (γ, α) rates modified by factors of 0.1 (solid line) and 10 (dashed line). The results for three times smaller and larger rates are indicated by squares and crosses, respectively.

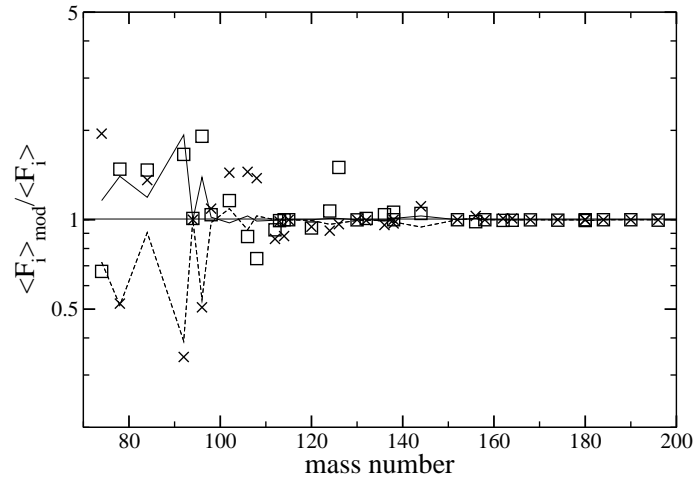


FIG. 13.— Same as middle panel of Fig. 10, but modifying only the (γ, p) rates of all p nuclei and their inverse (p, γ) rates by factors of 1/3 (solid line) and 3 (dashed line). The corresponding results of Fig. 10 are indicated by squares and crosses, respectively.

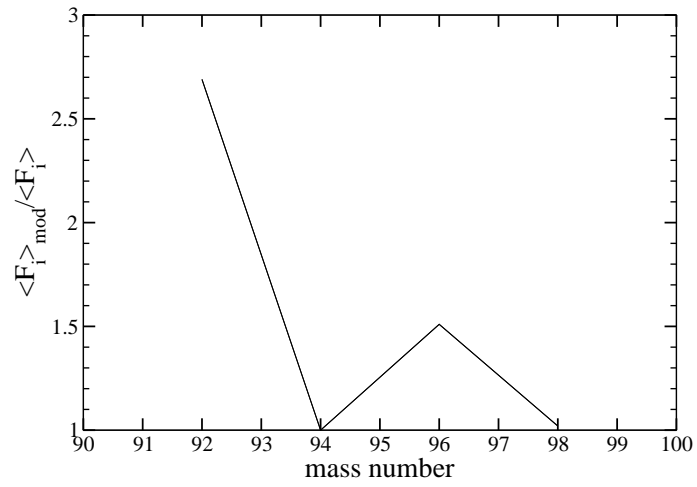


FIG. 14.— Ratio of the overproduction factors for the p abundances in the mass region $92 \leq A \leq 98$ obtained when reducing the (γ, p) destruction rates of ^{92}Mo , ^{94}Mo , ^{96}Ru , and ^{98}Ru by a factor of ten to the overproduction factors obtained with unchanged rates.

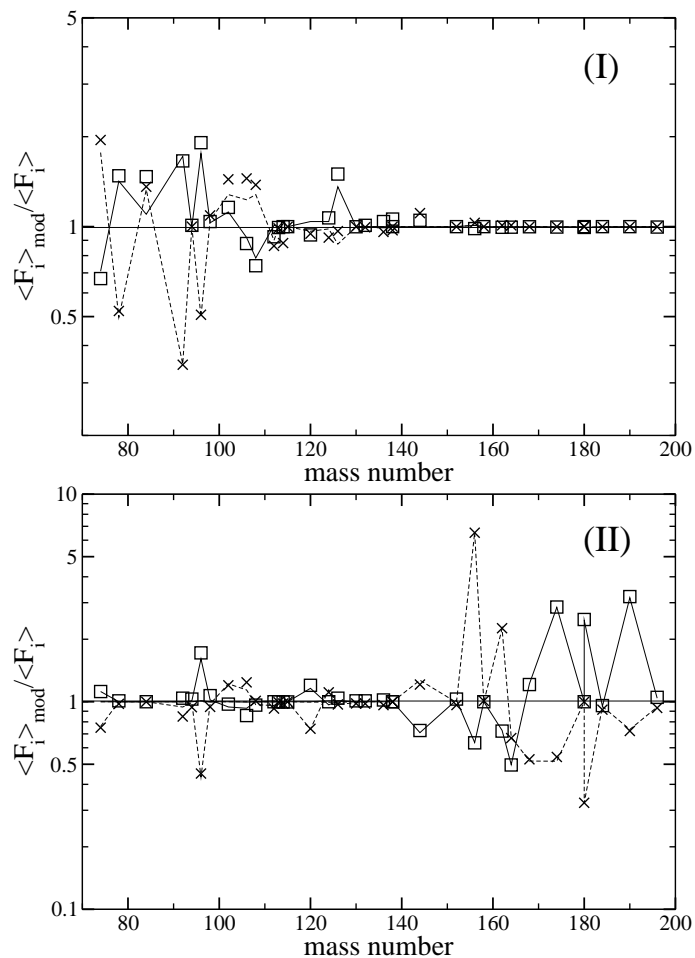


FIG. 15.— Influence of the selected reactions listed in Tables 2 and 3 compared to the results obtained by modification of all accepted HF-rates as shown in Fig. 10 (symbols). The top panel refers to the proton reactions of Table 2, and the bottom panel to the α reactions of Table 3. The effect of changes in the selected reactions is indicated by solid and dashed lines for reducing and increasing the rates by a factor of three, respectively. It is obvious that the selected rates are almost completely accounting for the response of the p -process network to reaction rate uncertainties.

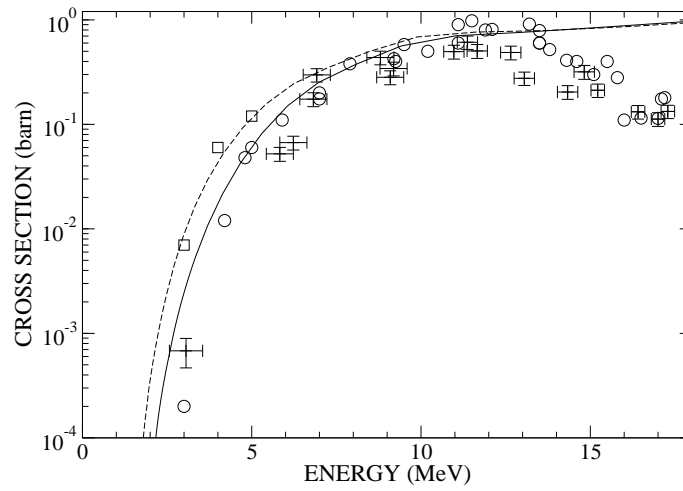


FIG. 16.— Cross section data for two sets of $^{75}\text{As}(p,n)$ measurements ((squares) (Kailas et al. 1979), (circles) (Mushtaquet et al. 1988)) in comparison with Hauser Feshbach predictions (solid line) (Rauscher & Thielemann 2001). Also shown is the experimental cross section of $^{85}\text{Rb}(p,n)$ ((crosses) (Kastleier et al. 2002)) in comparison with Hauser Feshbach predictions (dashed line) (Rauscher & Thielemann 2001).